Exploring mechanochemical parameters using a DoE approach: Crystal structure solution from synchrotron XRPD and characterization of a new praziquantel polymorph

A new praziquantel polymorph discovered by means of a DoE approach: crystal structure solution from Synchrotron XRPD and characterization

Debora Zanolla,[1] Beatrice Perissutti,[1] Paolo Cerreia Vioglio,[2] Michele R. Chierotti,[3] Lara Gigli,[4] Nicola Demitri,[4] Nadia Passerini,[5] Beatrice Albertini,[5] Erica Franceschinis,[6] Jennifer Keiser, [78] Dario Voinovich[1]*

[1]University of Trieste, Dept. of Chemical and Pharmaceutical Sciences, P.le Europa 1, Trieste, Italy
[2]Aix-Marseille Université, CNRS, ICR (UMR 7273), 13397 Marseille cedex 20, France
[3]University of Torino, Dept. of Chemistry and NIS Centre, V. Giuria 7, Torino, Italy
[4]Elettra-Sincrotrone Trieste, S.S. 14 Km 163.5 in Area Science Park, Basovizza–Trieste, Italy
[5] University of Bologna Dept. of Pharmacy and BioTechnology, Via S. Donato 19/2, Bologna, Italy
[6]University of Padova Dept. of Pharmaceutical and Pharmacological Sciences, via Marzolo 5, Padova, Italy
[7]Swiss Tropical and Public Health Institute Helminth Drug Development Unit, Dept. Medical Parasitology and Infection Biology, Basel, Switzerland
[8]Universität Basel, Petersplatz 1, P.O. Box, CH-4001 Basel, Switzerland

---

** Corresponding author:*

Beatrice Perissutti: E-mail address: bperissutti@units.it;

Tel. +39 040 558 3106;ORCID 0000-0002-5766-4014

ABSTRACT

To explore the experimental design space (in terms of frequency and time of milling) nearby the milling parameters of Praziquantel (PZQ) polymorph B formation, a rotated Doehlert matrix was employed. Three experimental responses were evaluated on ground samples: two quantitative ones, the median particle size by Laser Light scattering (LLS) and the drug recovery by HPLC, and a qualitative dependent variable, the obtained PZQ crystal form,characterized through X-Ray Powder Diffraction (XRPD) and confirmed by Differential Scanning Calorimetry (DSC) and Thermogravimetric analysis (TGA). The temperature inside the jars during the milling process was continuously monitored by using jars equipped with temperature sensors, allowing to consider the solid state obtained in each experimental point in the light of the specific temperature of the process. This explorative analysis led to the discovery of a novel PZQ polymorph, named Form C, which was produced without degradation and then fully characterized also by means of Synchrotron XRPD, Polarimetric, FT-IR, SS-NMR, ESEM, saturation solubility and *in vitro* dissolution rate analyses. Crystal structure was solved from XRPD data and its geometry was optimized by DFT calculations (CASTEP). Finally, Form C activity against adult schistosoma mansoni in comparison to raw PZQ was tested in vitro, and its physical stability was checked. The new polymorph, crystallizing in space group I2/c, physically stable for 2 months, showed a m.p. of 106.84°C and displayed excellent biopharmaceutical properties (water solubility of 382.69±9.26 mg/l and fast dissolution: t90% of about 50 min), while preserving an excellent activity against adult schistosoma mansoni.

KEYWORDS:

Praziquantel; crystalline polymorph; mechanochemistry; Doehlert design; median particle size; drug recovery; solubility; bioactivity; crystal structure solution; GIPAW; thermojars.

INTRODUCTION

Praziquantel (PZQ) (which structure is reported in Figure 1) is the only drug marketed for treatment and in so-called preventive chemotherapy against *Schistosoma* spp. infections [1]. According to the Biopharmaceutics Classification System, PZQ belongs to the class II drugs, because of its high permeability and low solubility (0.4 mg/mL) [2, 3]. PZQ has also a high first pass metabolism (1-3 h), which converts the active R-PZQ into inactive metabolites very rapidly [4,5]. Therefore a high dosage (40 mg/Kg) is required to be effective by using big tablets [6]. This fact, combined with the disgusting taste of the drug, results in a limited compliance to the therapy, especially in children, representing more than 50% of patients. To overcome these problems, a crystalline polymorph of PZQ, which is based on the commercial racemic PZQ and obtained by neat grinding in a vibrational mill in suitable process conditions, was recently prepared [7]. Its structure was solved from the synchrotron XRPD pattern resulting in a centrosymmetric *C*2/*c* unit cell with one crystallographically independent molecule. Form B, indexed as TELCEU01 (CCDC 1557658) [7] in the Cambridge Structural Database [8], has double solubility and intrinsic dissolution rate (IDR) in comparison with raw PZQ [7], and similar in vivo efficacy to the standard PZQ [9].

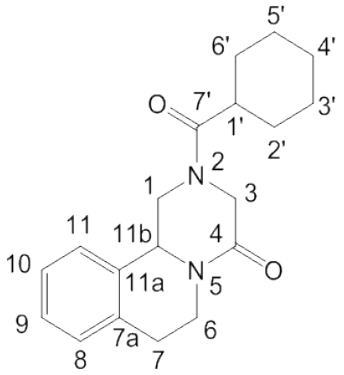

Figure 1. Chemical structure of Praziquantel (PZQ) with atom numbering.

In this paper, the nearby milling conditions of Form B production will be deeply investigated by using a design of experiments (DoE), and in particular a Doehlert design. This design, proposed by Doehlert in 1970 [10], is an experimental design for second order models providing a uniform shell design. The Doehlert matrix, derived from the simplex optimization, has been frequently used in the optimization processes of many fields because of the uniformity of the points in the experimental domain that permits to identify a response surface by means of a minimum of experiments [11,12]. The comparison among other second-order designs (such as Central Composite Design or Box–Behnken) has showed that the Doehlert design is the most efficient of the three [13]. The Doehlert matrix has been widely used for optimization of analytical or

extraction methods [14,15]; in materials science many of the papers reporting the use of a Doehlert matrix involve optimization or explorative analysis of process and/or formulation variables, and quality control in the development of pharmaceutical product [16-18]. Not yet documented is the use of such designs in the search of new polymorphic forms, and generally very poorly documented nowadays is the use of DoE approach in crystal engineering [19] and mechanochemistry [20,21]. In this case the Doehlert design will be applied to explore the experimental design space of Form B formation by neat grinding, defined by 2 process variables: time and frequency of milling. In fact, while the rules which decide the nature of transformations induced by milling are not yet clearly established, it seems that the main physical parameters involved are milling intensity and milling temperature (both related to frequency and duration of the milling) [22].

The Doehlert design can be proposed in the classical hexagonal form or in its rotated form, where each point is characterized by different values of the selected variables [11], the latter being the experimental design chosen for this work. PZQ crystal form at the end of the process was considered as qualitative experimental response of the explorative analysis. The median particle size and the drug recovery of the ground samples were also studied as a function of the variation of time and frequency of milling. Then the solid state obtained in each experimental point was considered in the light of the temperature measured in special thermojars in different milling conditions.

This explorative analysis led to the discovery of an additional PZQ anhydrous polymorph, namely Form C, which was obtained in quantitative yield. The new form C was fully characterized by means of Differential Scanning Calorimetry (DSC), Thermogravimetric analysis (TGA), Synchrotron X-Ray Powder Diffraction, (XRPD) Polarimetric and High performance liquid chromatography analyses (HPLC), solid-state NMR (SSNMR) and FT-IR studies. Particle morphology was studied by ESEM. Crystal structure was solved from XRPD data and its geometry was optimized by GIPAW-DFT calculations. Water saturation solubility and in vitro dissolution studies were carried to test biopharmaceutical properties. Finally, its activity against adult *Schistosoma mansoni* in comparison to PZQ was tested in vitro, and its physical stability checked over a period of 4 months.

2. Materials and Methods

2.1 Materials

Praziquantel (PZQ) Ph. Eur. grade ((11bRS)-2-(Cyclohexylcarbonyl)-1,2,3,6,7,11b-hexahydro-4-H-pyrazino[2,1-a]isoquinolin-4-one) was a kind gift from Fatro S.p.A. (Bologna, Italy). PZQ impurity A (2-Benzoyl-1,2,3,6,7,11b-hexahydro-4-H-pyrazino[2,1-a]isoquinolin-4-one) and impurity B (2-Cyclohexanecarbonyl-2,3,6,7-tetrahydro-pyrazino[2,1-a]isoquinolin-4-one) were Ph. Eur. grade and obtained from Endotherm Gmbh (Saarbruecken, Germany). HiPersolv Chromanorm Methanol (Ph. Eur. for HPLC Gradient Grade) and Ethanol (Ph. Eur.) were acquired from Sigma Aldrich.

2.2. Explorative analysis using Doehlert experimental Design

Starting Praziquantel (PZQ form A, indexed as TELCEU in the Cambridge Structural Database (CCDC 896767) [23] was milled on its own, by neat grinding, in a vibrational mill-Retsch MM400 (Retsch GmbH) which was equipped by 2 screw-type zirconium oxide 35 ml jars. Based on earlier studies [7, 24], a powder amount of 0.8 g was introduced in each milling jar, three spheres of 15 mm (weighing 10.72 g each) were used as milling media and a ceramic material like zirconium oxide was selected for the jars and spheres, allowing for a high energy input.

Time (x_1) and frequency (x_2) of milling were varied according to an experimental design. In particular, the experimental design space around Form B formation (TELCEU01)[7] was explored by means of a rotated Doehlert matrix, designed using NEMRODW software [25]. The conditions of polymorph B formation (240 min at 20 Hz) were chosen as the central point of the Doehlert matrix. The experimental domain and the experimental plan are shown in Table 1. For two variables, the Doehlert design consists of one central point and six points forming a regular hexagon, and therefore situated on a circle; three additional points were considered inside the design space, to reach a total number of 10 experiments. The experiments were carried out in random order (also reported in same table) and each milling trial was simultaneously carried out in both jars. The room temperature was thermostated at 22°C. As first experimental response of the explorative analysis (y_1) a qualitative dependent variable was chosen: the obtained PZQ crystal form (as it resulted from XRPD analysis, and confirmed by DSC and TGA analyses, according to paragraph 2.2.1.). In addition two quantitative variables were selected: the median particle size of the ground samples (y_2) (as determined by Laser Light Scattering analysis, according to paragraph 2.2.2.) and drug recovery after milling (y_3) (as determined by HPLC analysis, according to paragraph 2.2.3.).

After the treatment, the solid products were stored in the dark at 25°C in desiccators over anhydrous calcium chloride for further characterisation and processings.

2.2.1. Evaluation of (y_1): Solid state analyses

X-Ray powder diffraction (XRPD)

All ground samples were analyzed by X-ray powder diffraction using a Panalytical X'Pert Pro Diffractometer with Ni-filtered Cu Kα radiation (λ=1.5418 Å), the detector was a RTMS X'celerator. The preparation of the samples consisted in pressing about 20-30 mg of powder over a glass slide to have a flat surface. The data were collected in a 2θ range of 3-40 degree.

Differential Scanning Calorimetry (DSC)

Each sample was analyzed using a Mettler DSC TA 4000 (Greifensee, Switzerland) connected to a calorimetric cell Mettler DSC20 and using STARe software version 9.30 for data analysis. Prior to analysis the instrument was calibrated with Indium, Zinc and Lead for the temperature and with Indium for the

enthalpy quantification. In each analysis, about 2 mg of the sample was accurately weighted, placed in a 40 µl aluminum pan with perforated lid and heated 10°C/min from 30 to 160°C under air atmosphere.

Thermogravimetrical Analysis (TGA)

The thermogravimetric analysis was conducted using a Mettler Toledo TGA/SDTA851e: about 10-15 mg of the sample accurately weighted were placed in aluminum crucible (100 µL); then the heating was performed from 25 to 220°C, with a heating rate of 10°C/min under nitrogen atmosphere. To calculate the weight loss from the weight-temperature diagram, STARe software 11.00 was used.

Sample temperature continous measurement during grinding

The temperature inside the jar during the milling process was continuously monitored by using the ThermoJar set specific system (InSolido Technologies j.d.o.o., Zagreb, Croatia). It is composed by a PMMA jar equipped with a RTD (Pt-100) thermal sensor, a wireless infrared emitter with a dedicated logging system and software to collect, analyze and graphic the data (LogOS). The system is completed by another PMMA jar which is used to balance the milling system. In this way, the temperature measurements are specifically referred to the innert part of the jar, giving a description of its progress during time.The measurements were performed every second for 300 min grinding at 15-18-20-22-25 Hz, corresponding to the milling frequencies of the explorative analysis.

The powder temperature at the end of the process (300 min) both in the PMMA jars and in the conventional zirconium oxide jars was also measured using a 35XP-A Amprobe K-type thermocouple (Amprobe, Test Tools Europe, Glottertal, Germany).

2.2.2. Evaluation of (y2): Laser Light Scattering Analysis

The median particle size was measured by laser diffraction technique (Malvern Mastersizer Hydro 2000, Malvern Instruments, UK). The samples were dispersed in a small amount of distilled water containing 0.5% (w/w) of polysorbate 80 (Sigma Aldrich, Milan, Italy) and sonicated for one min. Sample dispersion was then poured in Mastersizer Hydro 2000 dispersion unit containing about 200 ml of water until the obscuration reaches a value between 10% and 20%. The analysis were performed in triplicate using a dispersion unit controller set to 1800 rpm. Particle size distributions were then calculated using a particle refractive index value of 1.700.

2.2.3. Evaluation of (y_3): Determination of drug recovery after milling

The content of PZQ was assayed in each ground sample by means of a reverse-phase HPLC-UV by adapting a method already reported in literature [26] and slighlty modified as previosly reported [7]; the system had two delivery pumps (LC-10 ADVP, Shimadzu, Japan), an autosampler (SIL-20A, Shimadzu, Japan) a UV-vis detector (SPD-10Avp, Shimadzu, Japan); the data were acquired at a fixed wavelength of 220 nm using

an interface (SCL-10Avp, Shimadzu, Japan) and analyzed with Ez-Star software; the column used was a Kinetex 5 μm C18 (150 x 4.60 mm, Phenomenex, Bologna). The mobile phase used was a mixture of methanol:water (65:35 v/v), purged at 1 ml/min. Injected volume was 20 μl. PZQ retention time was 5.5 min while the total run time for each sample was set at 12 min. Prior to analysis, a linear calibration curve with r^2=0.99996 was obtained for PZQ under these conditions using different concentrations of the drug from 0.3 to 10 mg/mL. Each day, a standard solution (with a concentration of 2.5 mg/L) was prepared by dissolving about 10 mg of PZQ accurately weighted in Methanol of HPLC grade (20 mL) and diluting the solution 1:200 with the mobile phase. Moreover, two additional calibration curves were obtained respectively for the relative impurity indicated in the Eur. Ph. (Ed. 8.0), impurity A (r^2=0.9993) and impurity B (r^2=0.9994), which were identified at the retention time of 3.45 min and 11.2 min. The reference solution did not report any of these impurities. Results were averages of four replicates.

2.4. Preparation of New Form C

Form C was obtained by neat grinding using the process conditions of experimental points EXP 3, 6, 8 and 10 of the experimental design. Nevertheless, the conditions of EXP 10 were taken as the standard ones, due to a sligthly higher crystallinity.

2.4.1. Evaluation of Form C

Polarimetric analyses

Optical rotations of the samples were measured on a Polarimeter Jasco P-2000 (Lecco, Italy), with a λ = 589 nm and a concentration of 1 g/100 ml in ethanol, according to the method reported in literature [27, 28] slightly modified by using ethanol in place of $CHCl_3$, as previously described [7].

Synchrotron X-Ray powder diffraction

Form C was analyzed using synchrotron XRPD at Elettra X-ray diffraction beamline (XRD1) [29] in order to obtain data suitable for the crystal structure solution and refinement. Diffraction patterns with improved resolution and signal to noise ratio have been obtained, compared to the conventional laboratory source results. Data were collected in transmission mode packing the powder in borosilicate capillaries with a diameter of 300 μm. Patterns were collected at room temperature using a monochromatic wavelength of 0.700A (17.71 KeV), 200*2000 μm^2 spot size on a hybrid-pixel Dectris Pilatus 2M area detector (Dectris Ltd., Baden-Daettwil, Switzerland). The patterns were then integrated using Fit2D program [30-31], after calibrating the hardware setup with LaB_6 standard reference powder (NIST 660a).

Solid-state NMR measurements

Solid-state NMR measurements of Form C were performed on a Bruker Avance II 400 instrument operating at 100.65 and 40.55 MHz for ^{13}C and ^{15}N nuclei, respectively. Cylindrical 4 mm o.d. zirconia rotors with a

sample volume of 80 μL were employed and spun at 12 (^{13}C) and 9 (^{15}N) kHz. All experiments employed the RAMP-CP pulse sequence (^{1}H 90° pulse=3.05 μs) with the TPPM ^{1}H decoupling with a rf field of 75 kHz during the acquisition period. 124 (^{13}C) or 5700 (^{15}N) transients were acquired with 3 (^{13}C) or 4 (^{15}N) ms of contact time and a relaxation delays of 20 s. ^{13}C and ^{15}N chemical shifts were referenced with the resonance of hexamethylbenzene (^{13}C methyl signal at 17.4 ppm) and NH_4SO_4 (^{15}N signal at -355.8 ppm with respect to CH_3NO_2).

GIPAW-DFT calculations

Periodic lattice calculations were performed using CASTEP [32] (Academic Release version 17.2) which exploits a plane-wave and pseudopotential approach within density functional theory (DFT).[33] The absolute chemical shieldings were calculated using the GIPAW algorithm [34] as implemented in the CASTEP code.

The geometry optimization and the NMR chemical shielding calculations were carried out employing the generalized gradient approximation (GGA) PBE exchange-correlation functional [35] with the semi-empirical dispersion scheme [36] TS [37] and ultrasoft pseudopotentials which were generated on the fly. The plane-wave cut-off energy was set equal to 700 eV, and the Brillouin zone was automatically sampled using a Monkhorst-Pack grid with a k-point spacing of 0.05 $Å^{-1}$.

The geometry optimization was performed starting from the structure of the Form C polymorph determined from synchrotron XRPD (space group I2/c, 376 atoms in the unit cell, Z' = 1), transformed in the equivalent space group C2/c (applying the transformation matrix [-1 0 -1, 0 -1 0, 0 0 1] to the 376 atoms in the unit cell, Z' = 1) for an easiest calculation set up. The experimental unit cell parameters were kept fixed during the optimization, as they were considered to be of acceptable quality. The convergence tolerances for the total energies, forces and displacements were set to $4.00.2•10^{-64}$ eV $atom^{-1}$, 0.015 eV $Å^{-1}$, and $5•10^{-4}$ Å 0.001Å, respectively. The refined structure was used in the subsequent chemical shielding calculation.

The absolute ^{13}C and ^{15}N isotropic chemical shieldings (σiso) were calculated using the same functional and parameters as those used for the geometry optimization. The plane-wave cut-off energy was set to 800 eV. The σiso were converted into the corresponding isotropic chemical shifts, δiso(calc), using the following conversion: δiso(calc) = σref − σiso. Here, σref is the reference shielding, obtained by plotting the experimental chemical shifts δiso(exp) against the GIPAW-calculated chemical shieldings. A linear regression model with slope constrained to (−1) was applied to find the best fit to the data (see Figures S1 and S2 in the Supporting Information). The value of σref is determined by the intercept with the y axis [38-39]. The obtained values of σref are 1712.2 ppm and 190.5 ppm for ^{13}C and ^{15}N, respectively.

FTIR Spectroscopy

FTIR spectrum of Form C was acquired at the solid state using a Perkin Elmer System 2000 FT-IR (Perkin-Elmer, Monza, Italy). The sample was mixed with anhydrous KBr (Anhydrous potassium bromide UVASOL, Sigma-Aldrich, Milan, Italy) in an agate mortar and then pressed with an hydraulic press for 2 min at 10 Ton to obtain homogeneous and transparent discs. The analysis was conducted form 400 to 4000 cm^{-1} with a resolution of 2 cm^{-1} and total scan number of 10.

Morphological analysis

The morphology of Form C was studied by an ESEM (Quanta 200 FEI) which permits the imaging of the substance with no prior specimen preparation. The analysis were performed under low-vacuum conditions in secondary electrons with a working distance of approximately 13 mm and an accelerating voltage of 20 kV. For comparison purposes, a JEOL JSM-5510LV (JEOL LTD, Welwyn Garden City, UK) Scanning Electron Microscope was used for imaging raw PZQ and Form B.

Determination of Drug Solubility

To determine the water solubility of Form C, saturated solutions were prepared in distilled water and kept under agitation in the dark for 48 hours at 20°C. Subsequently, the solutions were filtered with a membrane of 0.2 μm pore size, diluted 1:200 with the mobile phase (65% MeOH - 35% H_2O), injected in the HPLC instrument and analysed using the method previously described. For each sample, three different analyses were conducted and the average was taken as the corresponding data.

In vitro dissolution studies

Nine hundred ml of distilled water kept at 37 ±1°C were used as dissolution medium and uniformity conditions were ensured by an impeller (stirring rate 100 rpm). The determination of PZQ concentration was performed by using a fiber optic apparatus (HELLMA, Milano, Italy) connected to a UV-spectrophotometer (ZEISS, Germany) and managed with an user interface (Aspect Plus, Carl-Zeiss, Oberkochen, Germany). Prior to analysis, the peak of the UV-wavelength absorbance of PZQ was identified at 217.10 nm. The quantity of the sample to be introduced was calculated in order to achieve the sink conditions (with a total concentration ≤0.20 Cs), resulting in 10 mg and the quantity of PZQ dissolved was assayed *in continuum* for 60 min (one scan for minute). Each sample was analyzed in triplicate and the resulted mean±SD was considered as the final value.

Determination of in vitro activity against adult Schistosoma mansoni

In vitro studies were carried out in accordance with Swiss national and cantonal regulations on animal welfare (permission no. 2070) at the Swiss Tropical and Public Health Institute (Basel, Switzerland). Female mice (NMRI strain; weight ~ 20–22 g) were purchased from Charles River (Germany), kept under environmentally-controlled conditions (temperature ~ 25°C; humidity ~70%; 12-hour light and 12-hour dark

cycle) with free access to water and rodent diet and acclimatized for one week before infection. Cercariae of Schistosoma mansoni were obtained from infected intermediate host snails (Biomphalaria glabrata).

For the in vitro studies adult schistosomes obtained via dissection from infected mice were incubated in the presence of the test compounds at different concentrations (0.021-0.33 µg/ml) for up to 72 h. Phenotypes were monitored at several time points based on motility, viability and morphological alterations under an inverse microscope (Carl Zeiss, Germany, magnification 80x) [40]. Parasite viability values of treated and untreated worms obtained from microscopic evaluation were averaged (means ± standard deviation) using Microsoft Excel software. IC_{50} values were calculated using CompuSyn software.

Physical stability during storage and ulterior grinding

In order to check possible modifications of solid state within time DSC analyses of Form C were repeated for a period of 4 months. During storage time, the solid samples were stored in the dark in desiccators over anhydrous calcium chloride at 25°C. Also, the stability of Form C upon grinding for additional 60 min at 25 Hz was tested by DSC and XRPD.

RESULTS AND DISCUSSION

The experimental design space nearby the milling conditions of formation of PZQ polymorph B was examined with the help of a rotated Doehlert matrix to check the influence of operating parameters on the solid state and median particle size of PZQ, when neat ground by its own. The 10 experiments were performed in double (since the mills allows the set-up of two jars at the same time) varying time and frequency of milling, following the randomized order proposed in Table 1. The experimental responses are reported in Table 1, while a graphical illustration of the experimental design space, with the y_1 results in each experimental point, is presented in Figure 2. Finally, a picture with y_2 results will be reported in Figure 5.

Table 1. Doehlert design (2 factors) for neat grinding of PZQ: experimental domain, experimental plan, randomization and responses.

Independent variables		Lower level (coded -1)	Upper level (coded +1)
Milling time (min)	x_1	180	300
Milling frequency (Hz)	x_2	15	25
Dependent variables			
PZQ crystal form*	y_1		
Median particle size (μm)**	y_2		
Drug recovery after milling (%)***	y_3		

Exp.	Random order	X_1	X_2	Milling time (min)	Milling frequency (Hz)	y_1	y_2 (μm) (mean±S.D)	y_3 (%) (mean±S.D.)
1	6	0.966	0.259	298	21	B	68.00±3.29	99.01±0.14
2	2	-0.966	-0.259	182	19	*B*	71.85±5.03	98.32±0.34
3	10	0.259	0.966	256	25	C	55.46±4.01	99.04±0.02
4	3	-0.259	-0.966	225	15	M	40.44±4.57	99.64±0,04
5	9	0.707	-0.707	282	16	M	47.19±3.09	99.32±0.16
6	4	-0.707	0.707	198	24	*C*	58.06±0.48	99.38±0.11
7	1	0.000	0.000	240	20	B	77.44±3.99	99.55±0.05
8	5	-0.433	-0.250	214	19	*C*	54.17±5.22	99.71±0.13
9	7	0.433	-0.250	266	19	M	40.80±0.34	99.16±0.23
10§	**8**	**0.000**	**0.500**	**240**	**23**	**C**	**57.33±3.44**	**99.42±0.10**

*characterized by XRPD analysis and confirmed by DSC and TGA analyses. Letters in italic font indicate a solid product with reduced crystallinity degree (corresponding to ligth colors in Figure 2). The presence of Form B is reported as *B*, Form C as *C*, while *M* correspond to mixtures of different crystalline forms and amorphous solid. ** determined by Laser Light Scattering; *** assessed by HPLC analysis;
§ process conditions taken as the standard ones for Form C

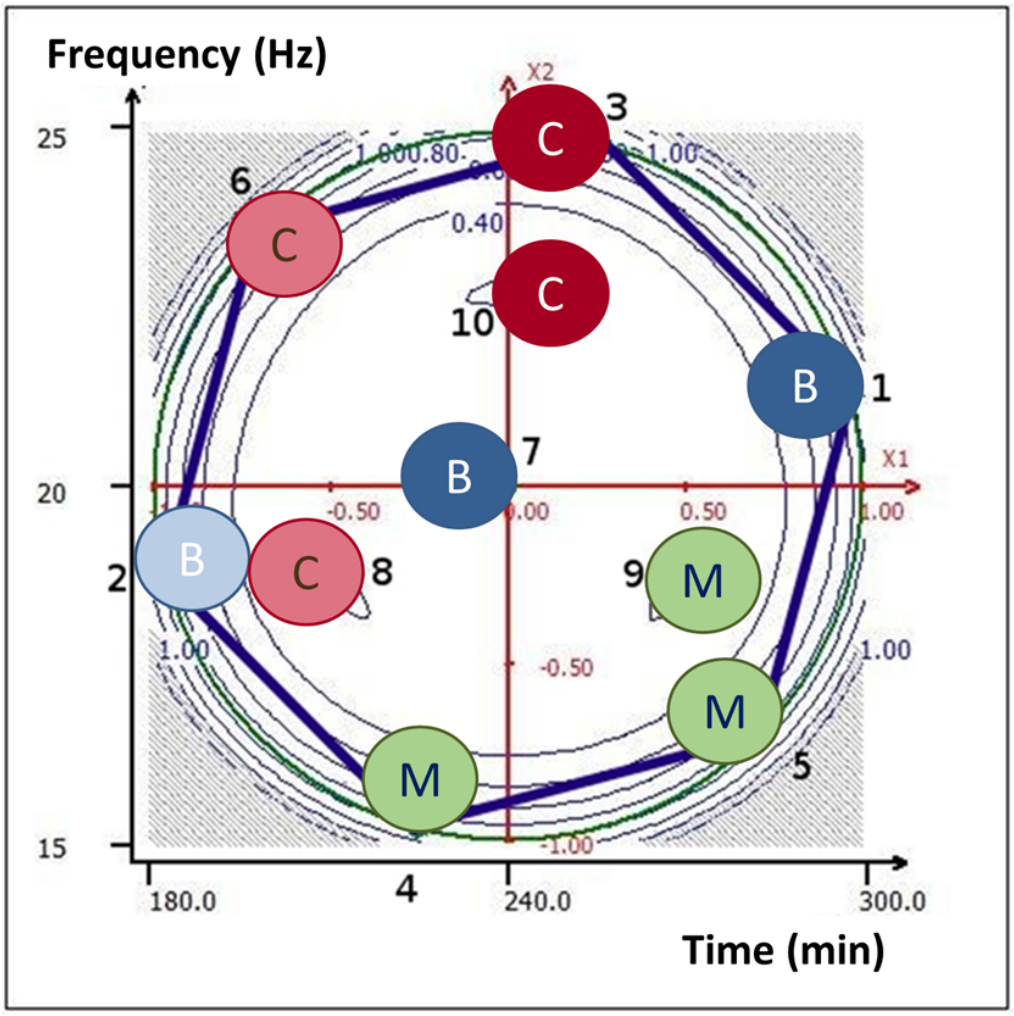

Figure 2. Distribution of the experiments in the rotated Doehlert design for two variables and different PZQ crystal forms otbained in each experimental point (y_1): Blue circles indicate Praziquantel Form B, Red circles Form C; ligth (blue and red) colors indicate a reduced crystallinity degree of Form B and C, respectively; Green cyrcles designate miscellaneaus of solid forms (mixture of amorphous and other crystal forms).

As clearly visible in Figure 2, it was possible to divide the 10 experiments in three groups, based on the solid state results (y_1). In the central zone of the hexagonal design space (EXP1, 2 and EXP 7 -central point of the design-) the presence of Form B, as the exclusive phase, with the characteristic XRPD pattern, endothermic peak at about 110 °C and absence of weigth loss upon heating, was attested. Furthermore, in correspondence of EXP 3, 6, 8 and 10, mainly located in the upper part of the design space, a different XRPD pattern was found and an unique melting peak at about 106-107° C without water loss, suggesting the presence of another unknown anhydrous phase (later referred as Form C). Finally, in EXP 4, 5 and 9, placed in the lower zone of the experimental domain, mixtures of starting/amorphous/ hydrate/ polymorphic PZQ were obtained.

In Figure 3 three XRPD patterns, representative of each group, are proposed; besides the complete list of XRPD patterns is depicted in Figure S3a,b,c and main DSC/TGA data are reported in Table S1.

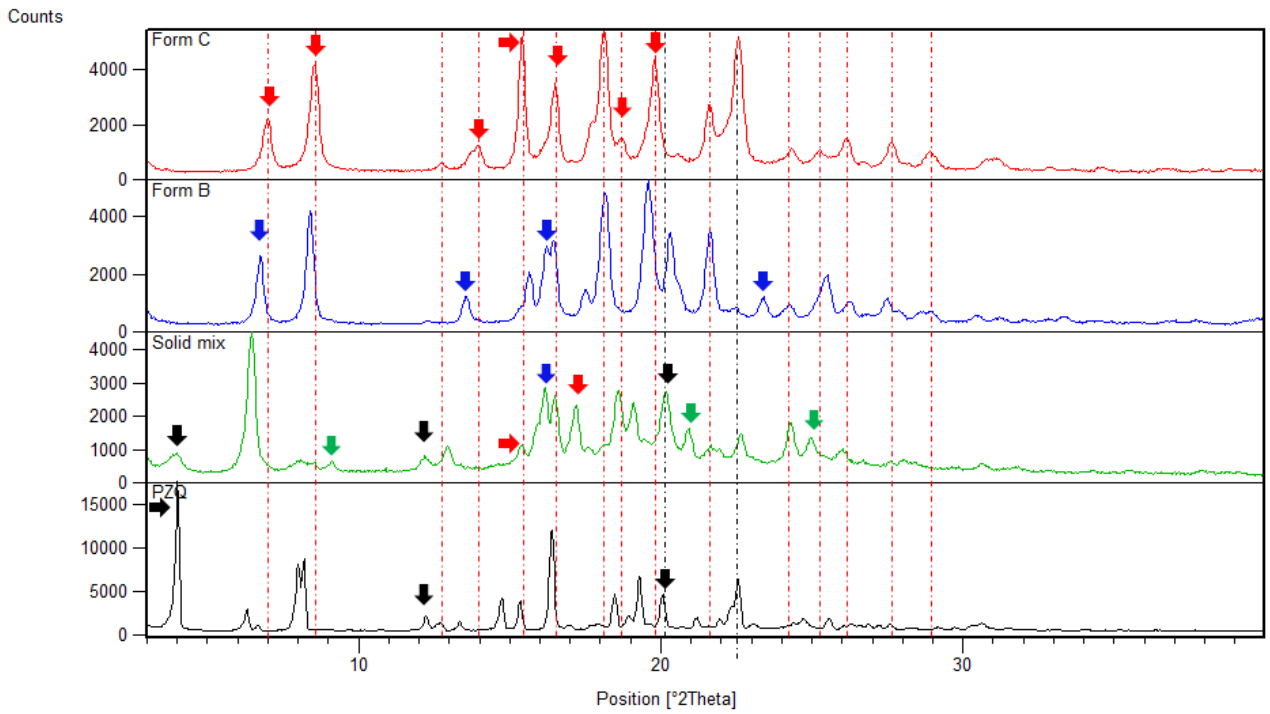

Figure 3 XRPD diffractograms representing the 3 solid states (y_1) found in the design space compared to commercial PZQ; arrows highlight peculiar signals of each solid form.

These results highligthed that PZQ solid state changes dramatically in response to little changes in time and frequency of milling. Indeed, as also showed in Figure 2, to reach a stable phase composition it is necessary a certain energy input. For example EXP 2, ground for a minor period of time, showed a reduced degree of crystallinity and lower reproducibility (of the results obtained from the two jars) than EXP 1 and 7 processed longer. Analogosly, in the second set of experiments (Form C), EXP 6 and 8, performed using lower frequency and/or milling time, did not provide constant results and the melting enthalpy was generally lower (these experiments are indicated with lighter colors in Figure 2). Finally, the bottom of the experimental domain (corresponding to lower mechanical energy input) corresponded to uncomplete solid trasfomations.

This set was in fact charcterized by multiple coexhisting phases: amorphous-nanocrystalline PZQ, traces of original PZQ (peculiar with respect to the other groups), hydrated phases (even small amounts of moisture in non-formally hydrated materials or in the laboratory environment can promote the formation of hydrate forms, as reported by several authors [41-44], and PZQ suffers from higroscopicity [45], and possibly an additional anhydrous polymorph not yet mentioned in the literature (having a weak melting endotherm at 98°C). As for this latter, given its limited concentration in the samples and the simultaneous presence of different solid phases herein, it was not possible to evince an exclusive pattern to distinguish an additional PZQ form. In addition, the weak endotherm may be also due to orginal PZQ form shifted to lower temperatures via the Gibbs-Thompson effect [46].

The measurement of powder temperature inside the jars in different milling conditions permitted to give additional explainations for the results of this explorative analysis for y_1. Powder temperature inside the jars was continously monitored (from 0 to 300 min) by means of special PMMA jars equipped by a temperature sensor. The results are shown in Figure 4. This was to check possible increase of temperature inside the jars (starting from a thermostated room temperature of 22°C), during the grinding process, since it is widely known that the impact and friction of the milling media with each others and the jars can induce an increase of powder temperature. The trend was the following: the temperature rapidly increased in the first 100 minutes of grinding, slowly reaching a plateau, even when milling for 5 hours. When grinding was performed at the highest frequency (25 Hz), the temperature reached after 180 minutes the maximum value of 39°C, and remained quite constant till the end of the process, while when grinding at 15 Hz the temperature never went beyond 33°C. These temperature data are in good agreement with the measurements performed with a thermocouple in the same vibrational mill [47] and by other authors [48]. As expected, the end temperatures detected in the jars made of zirconium oxide (having a different hardenss and heat capacity in comparision to PMMA) and in the PMMA jar were different, being slightly higher those measured inside zirconia jars (in particular, after 5 h at at 25 Hz and 15 Hz the reached temperature was ranging about 44°C and 35°C, respectively). Nevertheless the PMMA jars were useful in that they provided a description of temperature progress over time, otherwise impossible in the conventional zirconium jars.

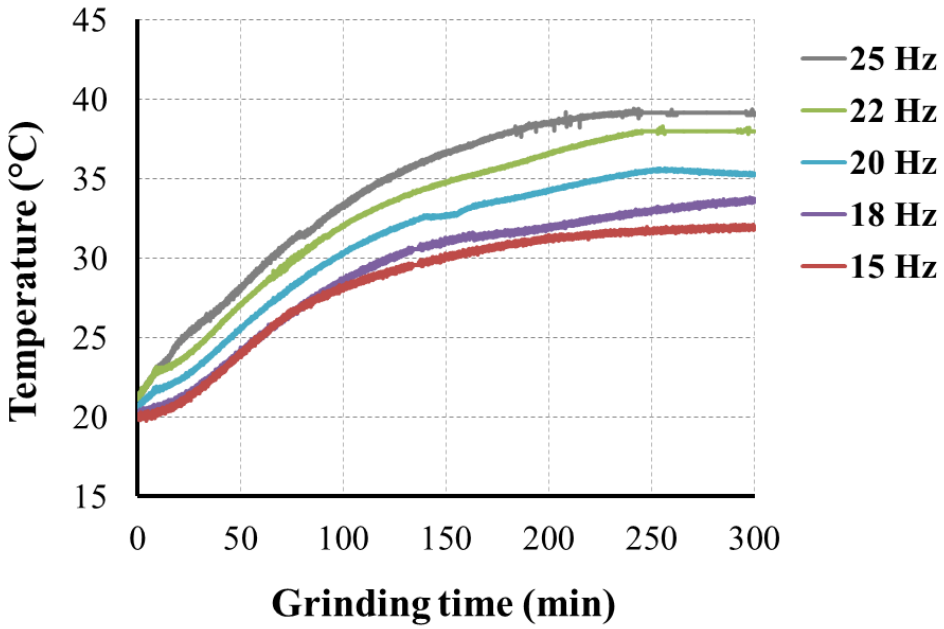

Figure 4. Temperature inside the jars during grinding at different frequencies measured using thermojars (according to paragraph. 2.2.1.).

A comparison of these process temperatures and PZQ glass transition temperature permits to draw some remarks of this explorative analysis in relation to y_1, remembering that amorphisation mainly occurs when milling is performed well below the glass transition temperature (T_g) of the system (the pure drug in this

case), while polymorphic transformations mainly occur when milling is carried out above [49]. As we already reported [47], glass transition of melt-quenched PZQ is 37.70 °C. In a milling-induced amorphous material, which migth correspond to an enhanced molecular mobility, this value may decrease [22,50]. This means that grinding at frequency 20-25 Hz permits to go well beyond Tg, whereas at 15 Hz powder temperature is ranging about Tg. This gives reason of the polymorphic outcome at higher frequency of milling (EXP 1, 3, 7, 10), where the temperature is around 40°C, and of the amorphous content detected in powder samples processed at lower time of milling (correponding to a temperature slightly lower than 40°C EXP 2, 6, 8). This also explains the high variability of the powder processed at lower frequencies (corresponding to EXP 9, 5, 4). In fact, in these experimental conditions, the powder temperature is in the PZQ Tg range, thus the behavior of the system highly depends on the milling conditions, increasing the uncertainty of the milling outcome [49].

Median particle size of the ground products (y_2)

As a second experimental response (y_2), the median particle size of the powder processed in different operating conditions was evaluated by LLS, with the aim of further characterisizing the solid products and of searching for a possible correlation between the different forms obtained by milling and the powder particle size. The median particle sizes of ground samples were comprised between 40 and 80 μm (as reported in Table 1 and depicted in Figure 5), differently from raw PZQ, having a median size of 23.99 μm with a slightly hinted bimodal shape distribution (see Figure S4 in Supplementary information). Even though a precise division could not be based on the particle size distribution, a certain correlation between crystal form and median particle size could be identified as following: the samples composed of Form B presented the biggest sizes, ranging around a d(0.5) of 72 μm while in the case of polymorph C the d(0.5) was smaller (around 56 μm). The lowest d(0.5) values were found in the case of the mixtures (around 42 μm). This was a further confirmation that depending on the process conditions, in this design space, the obtained solid products were divisible in three groups.

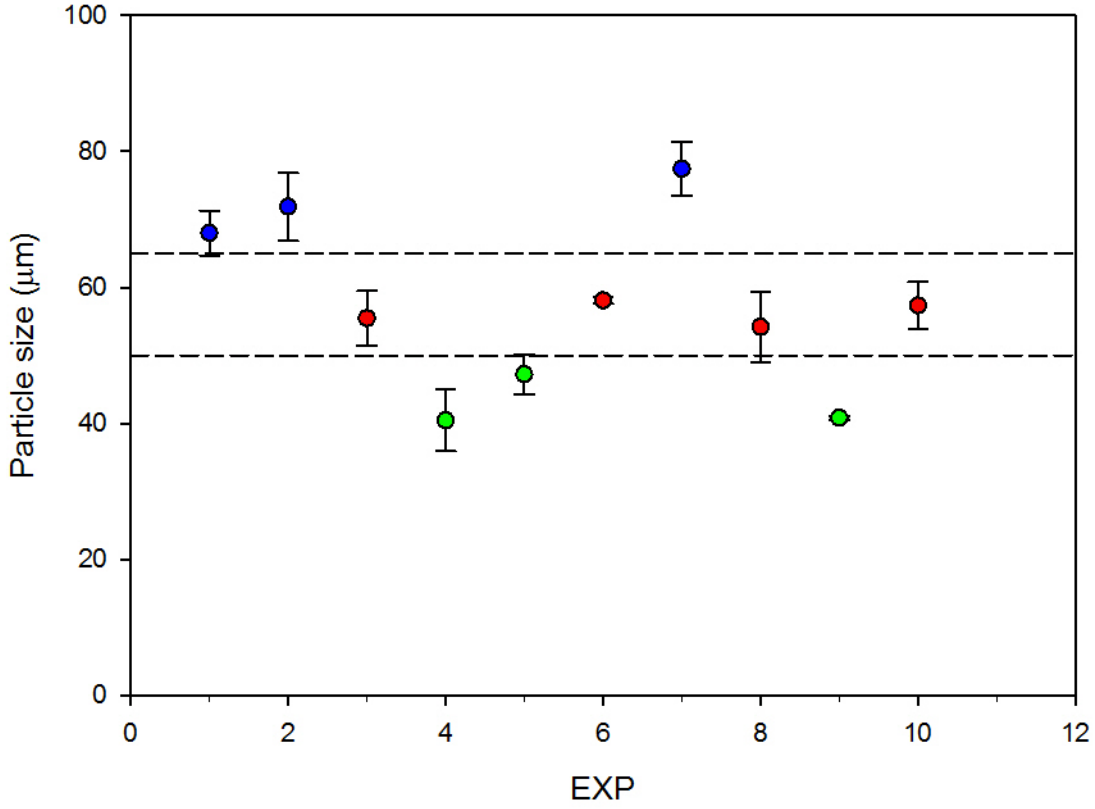

Figure 5. d(0.5) values and error bars (n=3) for the 10 ground samples (x axis reports the numbers of the experimental trial, blue circles indicate PZQ Form B, red circles Form C and green cyrcles designate mixture of solid forms (mixture of amorphous and other crystal forms).

Drug recovery after grinding PZQ by its own (y_3)

In the whole experimental domain, PZQ showed a degradation value of less than 1% with the only exception of EXP 2 (1.68%±0.34), as assessed by HPLC analysis and reported in Table 1 All ground samples were in accordance with the PZQ monograph in the Eur. Ph. (Ed. 8.0). This means that y_3 is almost constant in the studied design space and is not influenced by the variation of time and frequency of milling.

This also means that a high energy mechanical action (such as a protracted grinding for 182-298 min) on pure PZQ is capable of inducing changes in its physical state, either amorphisation or conversions between polymorphic crystalline forms, without producing significant chemical degradation. This is in contrast to its documented tendency to degrade when coground in presence of specific excipients [24,47,51]. In consideration of the different temperature detected in the jars (Figure 4) it is also evident that the heat is not the main responsible for drug degradation, in agreement to previous findings [47].

Evaluation of form C

The second part of this paper deals with the evaluation of Form C, which could be achieved in the conditions of EXP 3, 6, 8 and 10 of the experimental design. Nevertheless, the conditions of EXP 10 (240 min at 23 Hz) were taken as the standard ones, due to the highest crystallinity (see bold characters in Table 1). As anticipated in Table 1, in the case of for EXP 10 the drug recovery was of 99.42%.

At the DSC analysis, Form C shows the presence of a single well defined endotherm at 106.84 °C (ΔH=71.06 J/g), clearly distinct from Form B and commercial PZQ (Figure 6). No other thermal event was observed in this DSC curve. Form C anhydrous nature was testified by the lack of weight loss in the TGA analysis (reported in Table S1).

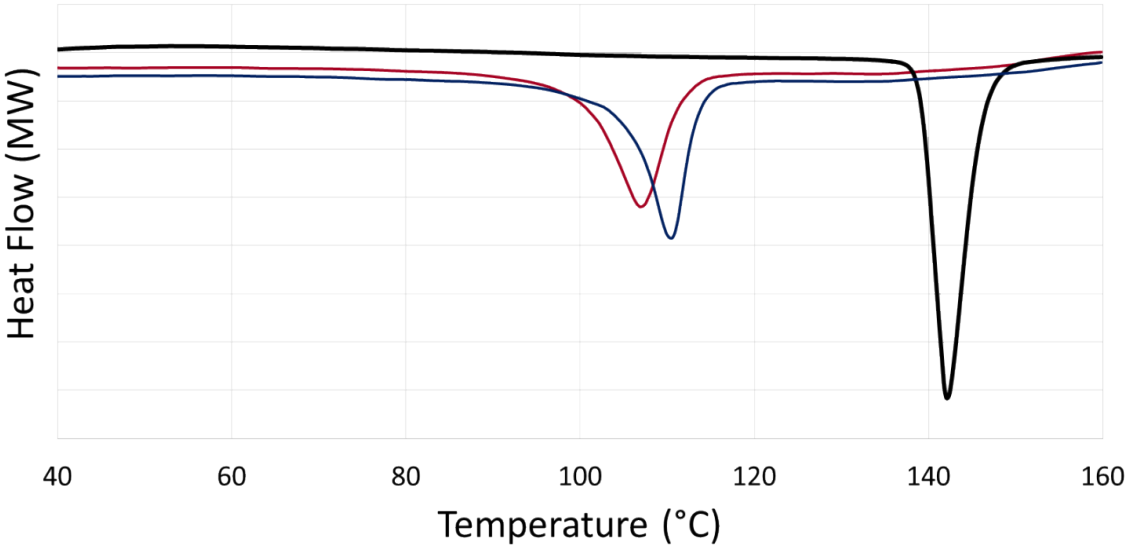

Figure 6. DSC traces of Form C (red), B (blue) and commercial PZQ (black).

Form C exhibited some differences in the habitus morphology (Figure 7) comparing to Form B and raw PZQ: the particles were agglomerated in groups, without any sign of the needle-shape like of raw PZQ or little whiskers of Form B, previously reported [7]. As also evident form these images, and in agrement with previous LLS findings, the neat grinding of PZQ in these process conditions led to the formation of agglomerates having dimensions larger than commercial PZQ particles'.

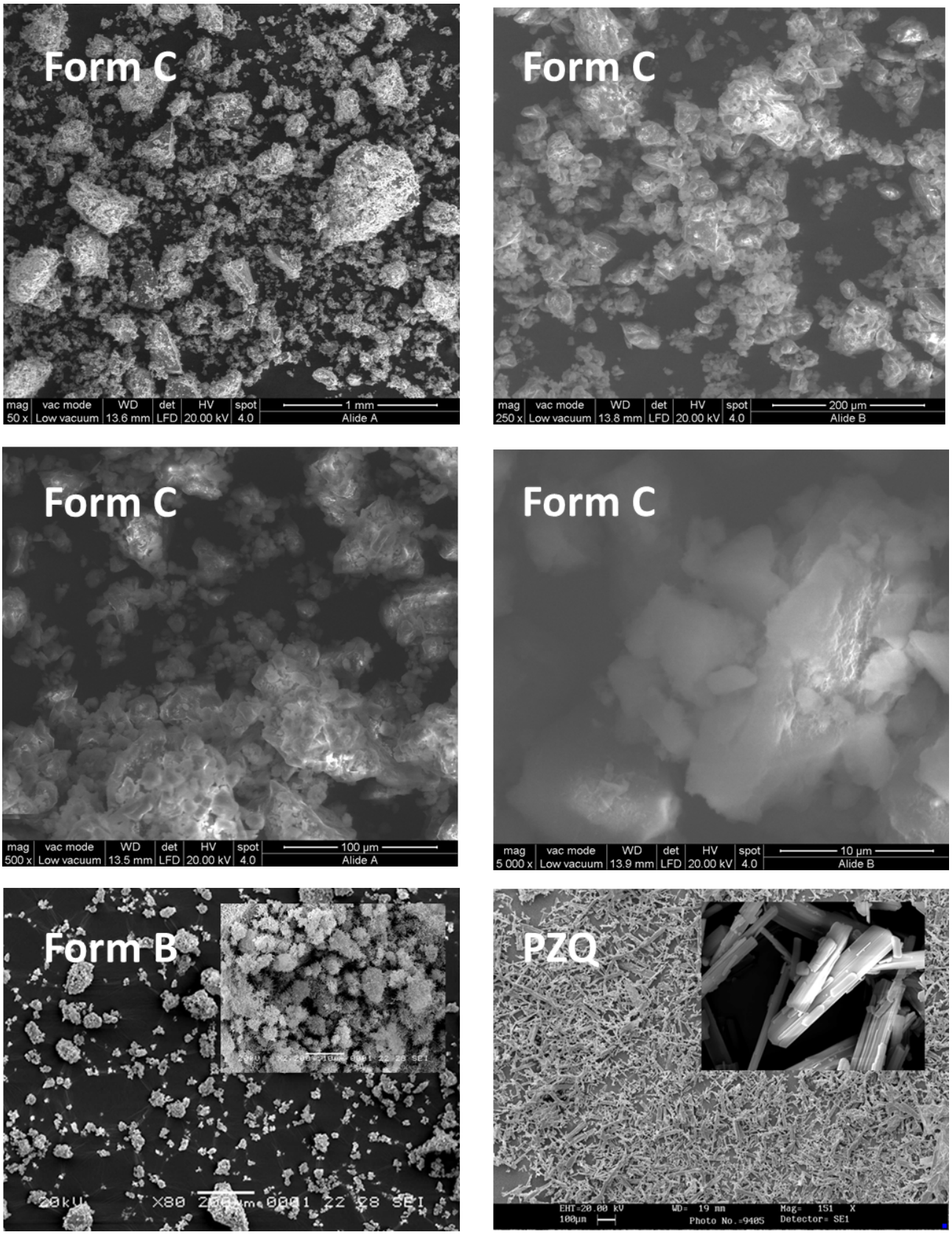

Figure 7. ESEM images of Form C (EXP 10) [magnification 50X, 250 x, 500x, 1000x] compared to Scanning Electron Micrographs of Form B (EXP 7) [mag. 80x, 2200x in the frame] and commercial PZQ [mag. 151x, 2200x in the frame].

The XRPD pattern of Form C, even if generally similar to Form B, was characterized by reflections at 6.98, 8.55, 12.76, 13.96, 15.42, 16.52, 18.12, 19.82, 21.62, 22.57, 26.15, 27.65 and 28.92° of 2θ as reported in Figure 3 (see vertical dotted lines), which highlight the differences between the forms.

The crystal structure of Form C was solved from the synchrotron X-ray powder diffraction data, depicted in Figure 8. The cell was indexed using EXPO2014 [52] and TOPAS V5 [53] was used for the simulated annealing process, using Form B as the model. The annealing process led to a Rietveld refinement with Rwp of 2.5%, also shown in Figure 8. The resulting centrosymmetric monoclinic cell (reported in Figure 9) has space group *I2/c* and the following parameters: a=22.02(2) Å, b=5.910(1) Å, c=26.980(2) Å, α=γ=90°, β= 109.765(4)°, density =1.26 g/cm^3 and volume 3304(2) Å^3. All the diffraction patterns obtained from different Form C batches showed the same profile and no additional spurious peaks have been found. CCDC 1878799 contains the supplementary crystallographic data for Form C. These data can be obtained free of charge from The Cambridge Crystallographic Data Centre via https://www.ccdc.cam.ac.uk/structures.

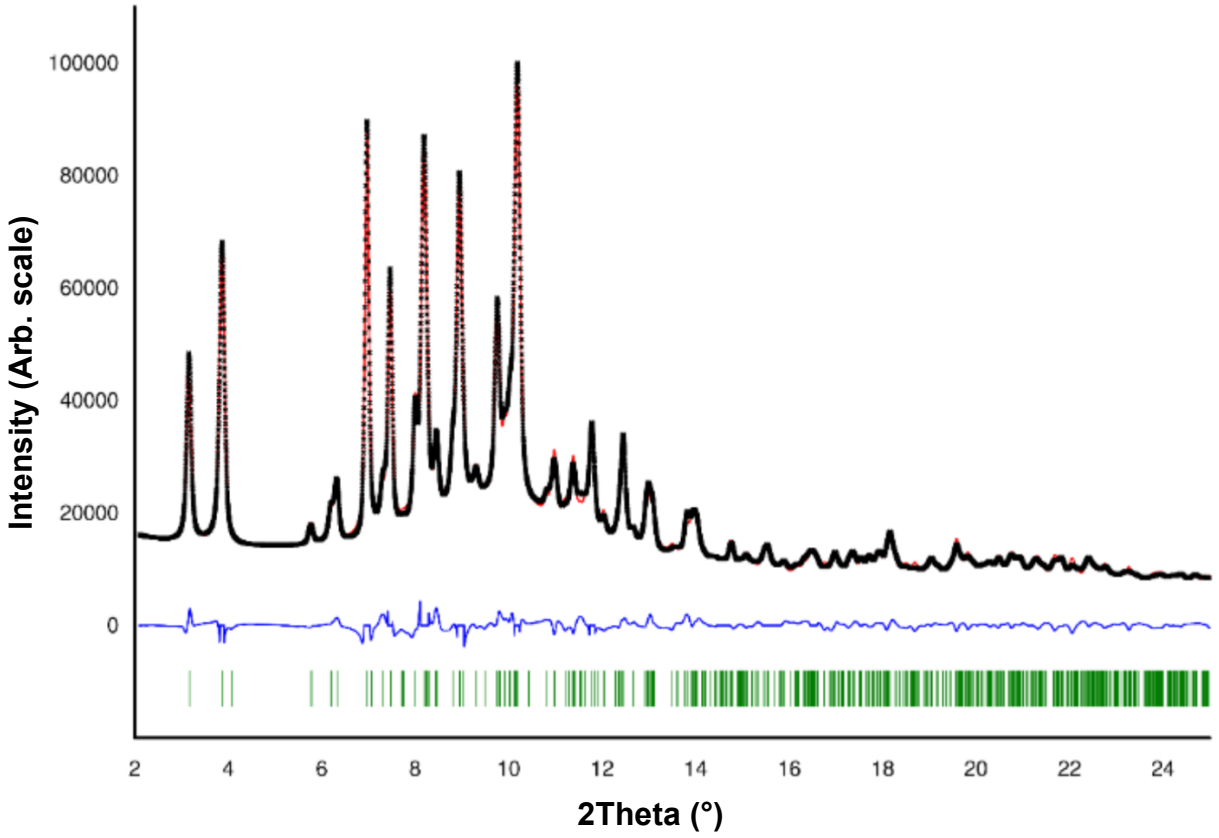

Figure 8. Rietveld refinement profile fit of Form C: in black the experimental pattern (collected using synchrotron radiation 0.700 Å), in red the calculated one. Residuals are displayed in blue and reflection ticks Atom: C….17 have been simulated from structure solution, and are reported in green.

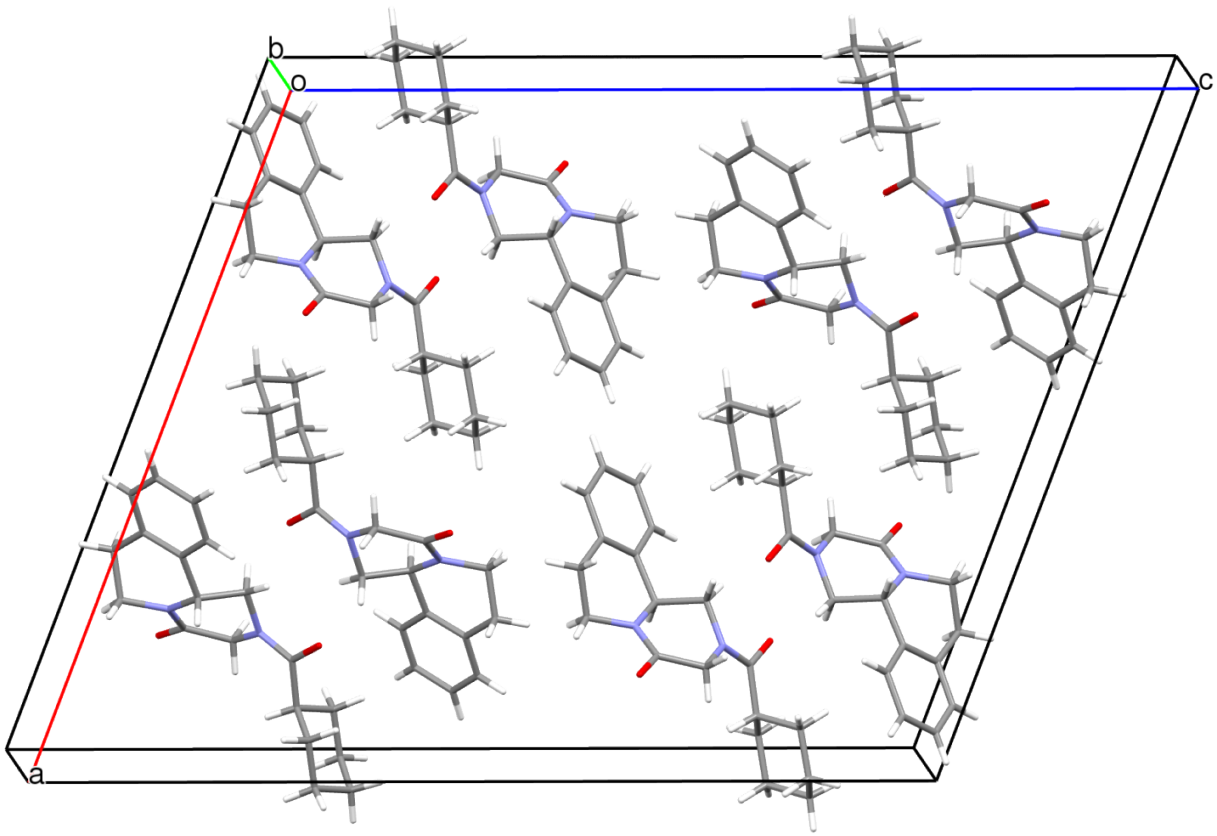

Figure 9. Capped stick representation of the proposed strucure and crystal packing for Form C racemic mixture. The monoclinic centrosymmetric unit cell hosts 8 molecules, one crystallographically independent, in a *I*2/*c* space group.

The cell has one crystallographically independent molecule in the asymmetric unit, as also confirmed in the ^{13}C CPMAS SSNMR spectrum (Figure 10) in which the differences between the packing of Form B and C are clearly visible. Even more evident the differences with commercial PZQ. In fact, similarly to Form B, in Form C only one set of resonances is visible, while raw PZQ is characterized by splitted signals, clearly evident in particular for the heterocyclic carbonyl at 164 ppm. The powder was also highly crystalline, as testified by very sharp peaks. ^{13}C chemical shift are listed in Table 2 with assignments and atom numering in chemical structure of PZQ is reported in Figure 1.

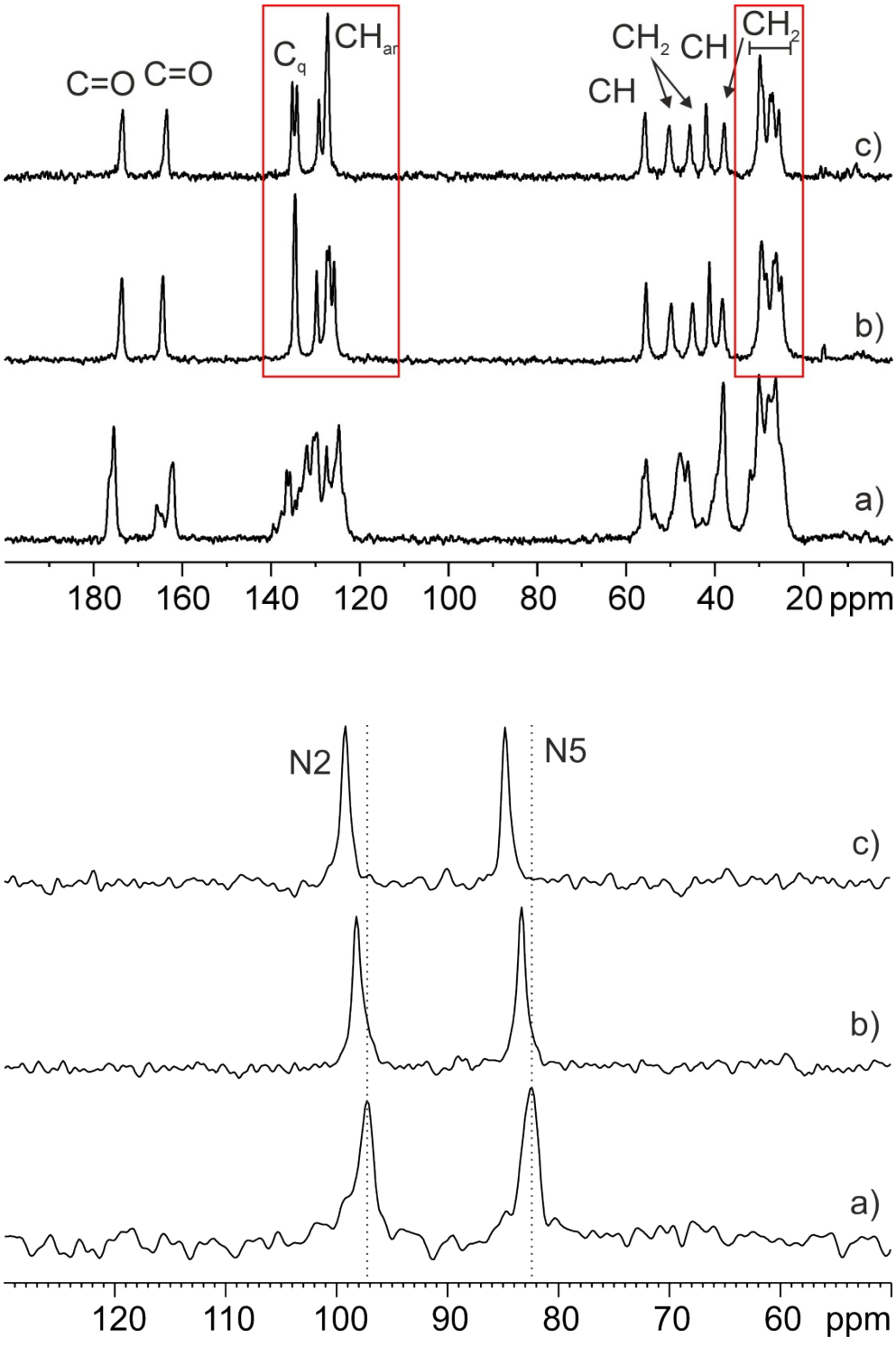

Figure 10. (top) ^{13}C (100.65 MHz) CPMAS spectra with principal group assignments of commercial PZQ (a) Form B (b), Form C (c) recorded at 12 kHz; (bottom) ^{15}N (40.55 MHz) spectra of commercial PZQ (a) Form B (b), Form C (c) recorded at 9 KHz.

Table 2. Experimental and calculated ^{13}C and ^{15}N isotropic chemical shifts for the polymorph Form C of PZQ, with the corresponding assignments for each site in the asymmetric unit. The GIPAW-calculated chemical shielding are also reported.

Atom	Group	^{13}C		
		δ_{iso}(exp) / ppm	δ_{iso}(calc) / ppm	σ_{iso} / ppm
7’	C=O	173.3	173.8	−2.6
4	C=O	163.4	163.1	8.2
7a	C_q	135.1	137.8	33.4
11a	C_q	134	136.8	34.5
8	$CH_{(ar.)}$	129.1	131.0	40.2
11	$CH_{(ar.)}$	127.5	129.4	41.8
10	$CH_{(ar.)}$	127.1	128.5	42.8
9	$CH_{(ar.)}$	n.a.[a]	127.9	43.4
11b	$CH_{(aliph.)}$	55.5	56.1	115.1
3	CH_2	50.1	49.3	121.9
1	CH_2	45.5	43.8	127.5
1’	$CH_{(aliph.)}$	41.8	40.5	130.7
6	CH_2	37.7	35.3	135.9
2'	CH_2	29.6	28.1	143.1
7	CH_2	29.1	27.4	143.8
6'	CH_2	27.4	27.3	143.9
3'	CH_2	26.8	25.5	145.7
4'5’	CH_2	25.4	24.5	146.7
5'4’	CH_2	n.a.[a]	23.4	147.9
			^{15}N	
2	N	84.8	84.5	106.0
5	N	99.2	99.5	91.0

[a]Resonances are indistiguishable.

GIPAW-DFT calculations were performed on the proposed crystal structure of Form C. In particular, the geometry optimization was initiated from the structure determined from the XRPD pattern (376 atoms) and the refined structure was used for the chemical shift calculation. As reported in Figure 11 the geometry-

optimized structure was almost completely superimposable with the one form the XRPD data and the simulated XRPD were identical (Figure 12).

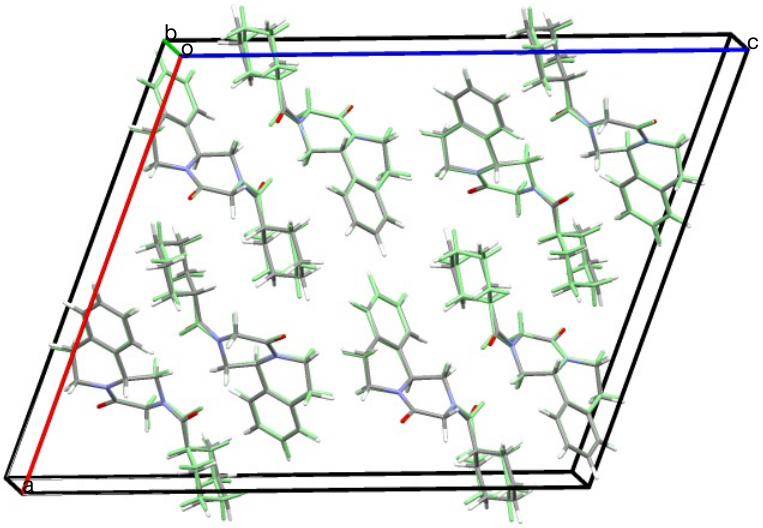

Figure 11. Overlay of the crystal structure of the polymorph C of PZQ from XRPD data and its geometry-optimized crystal structure by DFT calculations (in green). An all-atom root-mean-square value of 0.176 Å was obtained by the comparison of the two crystal structures, using the software Mercury (CCDC, v3.10) [54]. The positions of the hydrogen atoms were ignored.

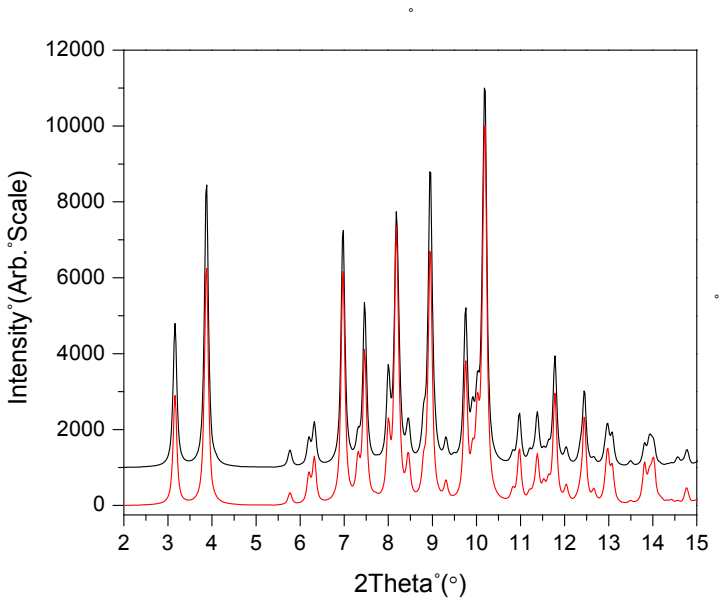

Figure 12. Comparison of the XRPD patterns of Form C crystal structure: in black, the simulation obtained from the DFT-optimized structure; in red, the simulated powder diffractogram of the Form C using the experimental crystal structure. Both simulations were carried out with Mercury by setting a wavelength of 0.700Å.

The calculated chemical shifts aided in assigning the resonances, and more importantly, they are a fundamental tool of the NMR crystallography approach since they provide correlation between the XRPD structure and the experimental one.[55-57] Indeed, we exploit them to reinforce the synchrotron XRPD data, by assessing whether the calculated ^{13}C, ^{15}N chemical shifts of the X-ray structure match the experimental ones that have been obtained from the above CPMAS experiments. Table 2 reports the assigned ^{13}C, ^{15}N resonances, as well as the corresponding calculated values. From the comparison of the experimental and computed ^{13}C chemical shifts, a root mean square deviation of 1.7 ppm is obtained. This overall value represents the agreement between the ^{13}C chemical shifts of the X-ray structure and those obtained experimentally. In an effort to rationalize this value, we note that Beran et al.[58] have recently assessed that GIPAW PBE ^{13}C chemical shifts can be calculated with a root mean square error of 2.2 ppm. Therefore, as our rmsd value is within this error, we can conclude that the X-ray determined structure correctly represent the crystal structure that corresponds to the SSNMR data. Finally, Figure 13 shows the graphical comparison between calculated and experimental ^{13}C chemical shifts: the data are linearly correlated with slope of 1.02 and a Pearson's correlation coefficient of 0.9996, thus demonstrating excellent agreement between calculation and experiment.

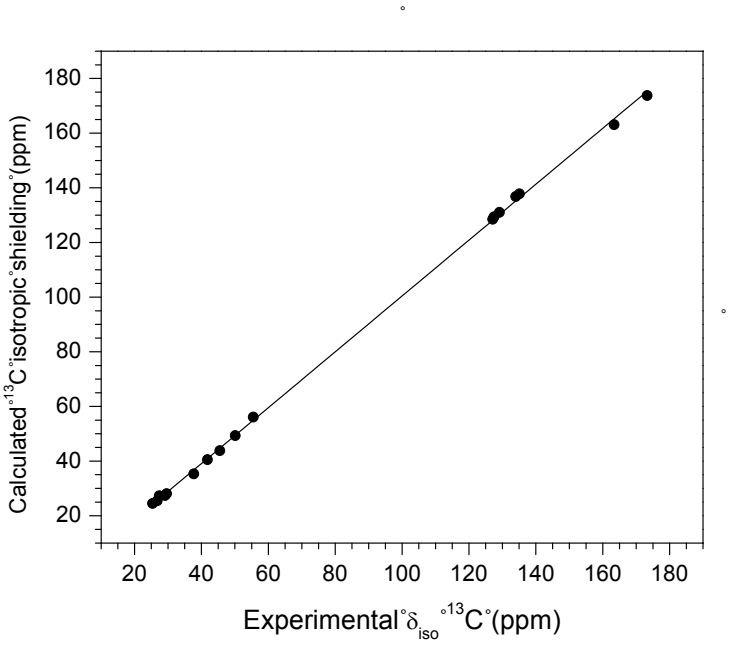

Figure 13. Plot of the GIPAW-calculated ^{13}C isotropic chemical shifts against the experimental ^{13}C isotropic chemical shifts. The line of best fit is $\delta_{iso}(calc) = 1.02[\delta_{iso}(exp)] - 1.80$, and the Pearson's correlation coefficient is 0.9996.

The crystal structure suggested a racemic nature for Form C, which was confirmed by polarimetric analysis, presenting an [α] of 0.0144±0.0295 (*n*=3) and XRPD.

The FT-IR spectrum of Form C, (Figure 14), was very similar to that of Form B, highlighting the close relationship between the polymorphs produced by neat grinding, while putting in light the differences with that of raw PZQ. In particular, for the region corresponding to the stretching of the carbonyl groups, indicated in the frame of Figure 14, also in the case of Form C, the conformers were in the *anti* position, as demonstrated by the lower frequency difference in ν(CO) between the carbonyl groups (1642 and 1631 cm^{-1}), whereas commercial PZQ showed the two signals at 1651 and 1626 cm^{-1} due to the *syn* conformation in accordance to previous literature [7, 59]. FT-IR spectroscopy was hence not useful for distinguishing between the two forms C and B, yet was helpful to discrimin easily both of them from commercial PZQ.

In addition, this analysis was a suitable tool because it attested the identical conformation of the two polymorphic varieties formed by dry grinding. This confirmed PZQ conformational flexibility [23] and supported the idea that, also in the case of PZQ, dry milling allowed a polymorphic conversion via an amorphous intermediate. It is in fact reported that amorphous PZQ possesses as well an anti-conformation of the two carbonyl groups [60]. This assumption is also in agreement with the mechanism of phase transition during mechanochemical reactions proposed by Shakhtshneider [61] and supported by several authors [42,43]. Moreover, it is worthy of note that even in a previous study of cocrystal formation by liquid assisted grinding, the PZQ isomer having anti orientation was shown to be preferred over the syn-isomer [23].

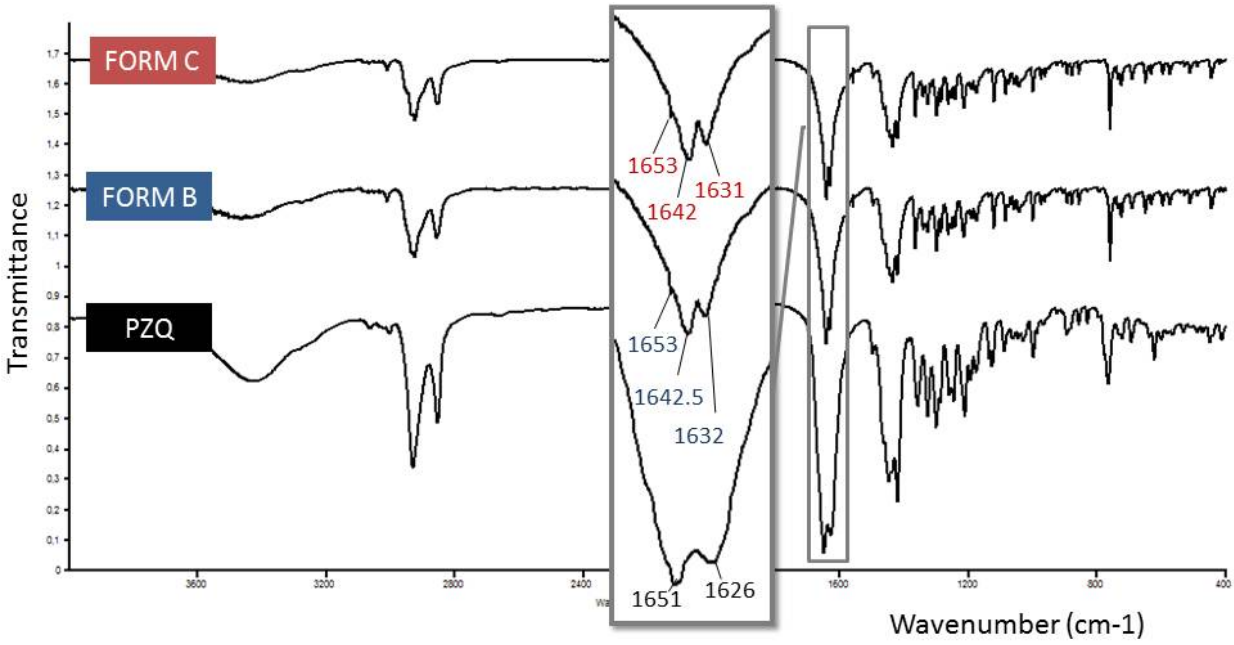

Figure 14. FT-IR spectra of the three PZQ polymorphic varieties

The water saturation solubility at 20°C of Form C was assessed and compared to raw PZQ and Form B, resulting in the most soluble form with 382.69 ± 9.26 mg/L (mean ±s.d.; n=5), while raw PZQ was 140.30 ±

9.25 mg/L and Form B 281.31 ± 8.32 mg/L (figure 15) . In agreement with these findings, also the dissolution performance of Form C at 37°C was better than raw PZQ, both in the entity and rate of dissolution, reaching the 90% of drug dissolved in about 50 min..

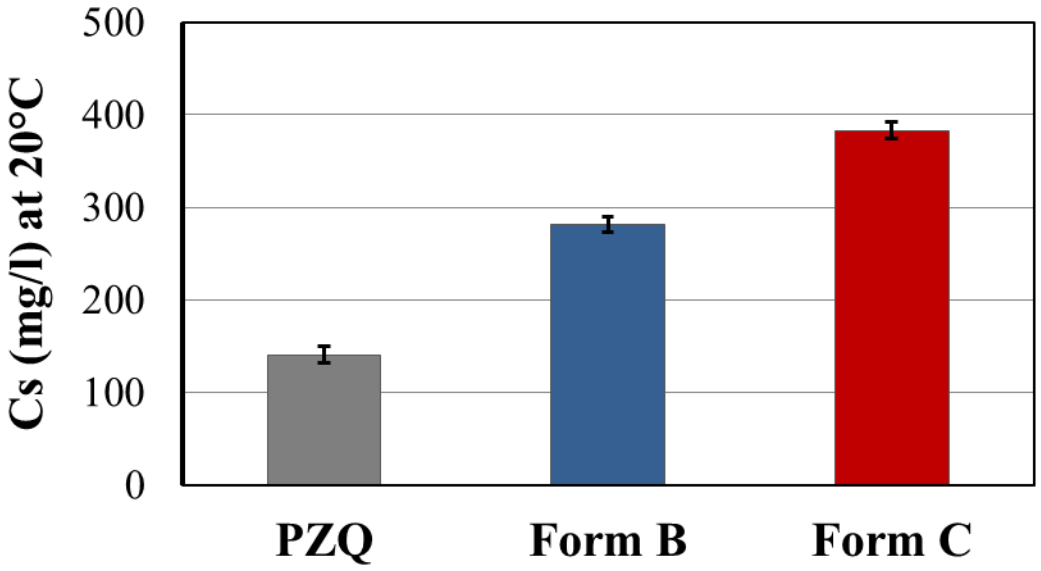

Figure 15. Water saturation solubility at 20°C of the anhydrous forms of PZQ.

In vitro antischistosomal activity of Form C (against Schistosoma Mansoni adult) was then tested, resulting in an IC_{50} of 0.21464 μM (r= 0.97485 μM) after 72h, which is similar to PZQ's one (0.1. μM) [62]. This testifies the maintaining of the Form C activity, even though the extensive grinding performed for its production. This fact also attests that the conformational polymorphism does not affect its activity, in a similar way to what has already been found in the case of form B [7].

Form C was unchanged for 2 months, while after three months it started to slowly recrystallize in PZQ commercial form (Figure 16), as visible from the weak endotherm detected at 135.81°C, with a downward shift due to the small crystallite size. This is quite typical of polymorphic forms produced by milling, which are almost always less stable than the starting (unmilled) form [22]. With respect to previously discovered Form B also produced by milling, which was stable for more than one year, the polymorph C is characterized by a dramatically lower physical stability. These findings are in agreement with its lowest melting point and highest water solubility among anhydrous PZQ polymorphs, and to the fact that metastable state generated by milling can recrystallize more or less rapidly upon storage.

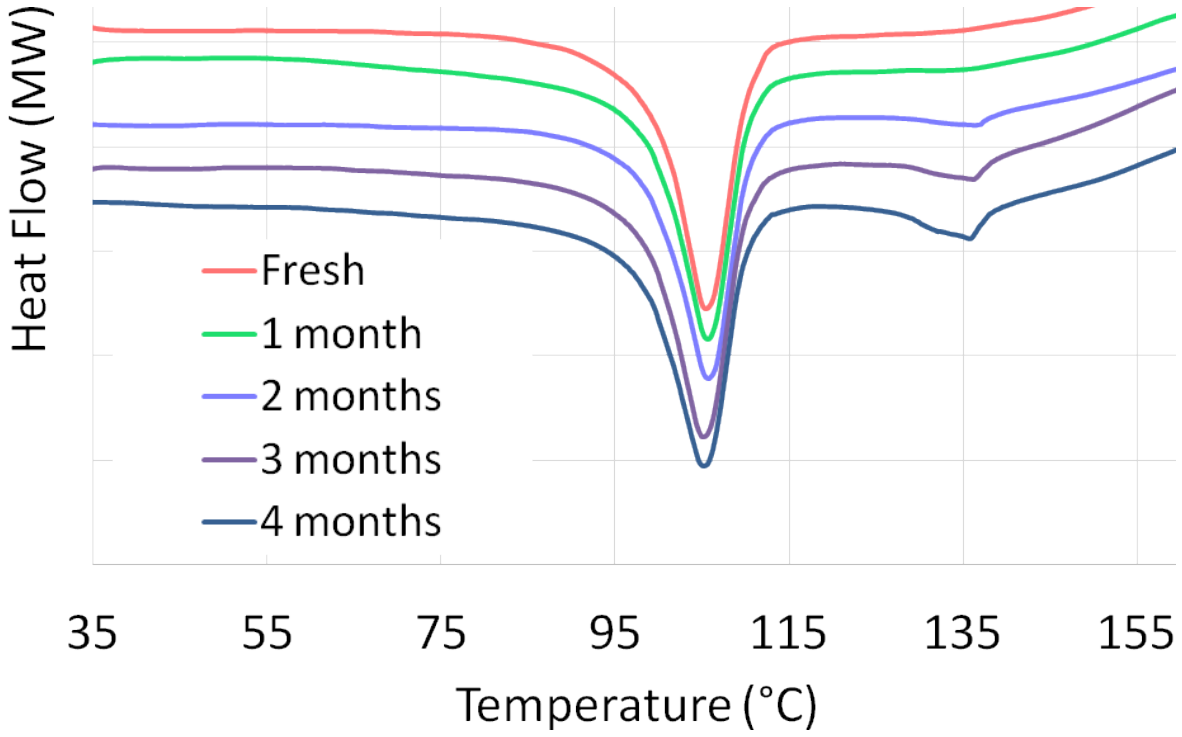

Figure 16. DSC curves of Form C on aging. From top to down: Fresh sample and samples after 1, 2, 3, 4 months.

When Form C was subjected to a further grinding for 60 min at 25 Hz, the DSC traces and XRPD pattern (Figure S5) also evidenced the formation of a certain amount of Form B in a sample mainly composed of Form C, still persistent. This means that, both on aging at ambient temperature (in a desiccator in the dark) and by milling again for further 60 min, the metastable form C converts into the most stable triclinic *P*-1 PZQ (CCDC 896767 [23]). Interestingly enough, the formation of Form B, which presumably is the metastable form closer to Form C according to Ostwal's rule of stages [63], is only possible by 4-5 h of milling only starting from commercial PZQ by non-interrupted continuous grinding. This confirms the general knowledge [22] that that milling process often induces a rich pattern of non-equilibrium transformations.

Conclusions

The performed work demonstrates that the application of DoE methodology in mechanochemistry is well suited for obtaining new polymorphic varieties, allowing the experimentalist to carefully consider every single factor affecting neat grinding reactions to drive the formation of the desired crystal form. Besides the

monitoring of the temperature inside the milling jars is an useful tool to understand and predict the end point of mechanochemical reactions. The new praziquantel polymorphic variety, Form C, found during the explorative analysis, represents the third anhydrous crystal of this drug. It can be obtained by neat grinding of the drug by its own, without any solvent addition, and it is otherwise inaccessible by conventional crystal engineering methods. The multidisciplinary approach applied for its characterization has permitted to successfully solve its crystal structure from Synchrotron XRPD, to propose a mechanism of formation induced by mechanochemical conditions and to highlight the strengths and weaknesses of the Form C of Praziquantel, the drug of choice for the Schistosomiasis treatment.

Aknowledgements

This research did not receive any specific grant from funding agencies in the public, commercial, or not-for-profit sectors. PCV thanks Dr. G. Mollica for valuable discussion on GIPAW-DFT calculations. BP thanks Alice Cerniz and Anna Candido for preparation of the samples.

Supporting information

Plot of the experimental ^{13}C and ^{15}N chemical shifts against the GIPAW-calculated ^{13}C and ^{15}N chemical shieldings (σiso), respectively; XRPD patterns and DSC/TGA data of all samples included in the explored experimental domain; particle size distribution of commercial PZQ; physical stability of Form C upon milling.

Crystallographic information file (CIF) for Form C, embedding the measured and calculated profiles. (Structure factors are available from CCDC - CCDC 1878799).

Conflict of interest

The authors there are no conflicts of interest associated with this publication and there has been no significant financial support for this work that could have influenced its outcome.

References

[1] D.G. Colley, A L Bustinduy, WE Secor, C H King, Human schistosomiasis, Lancet 383 (2014) 2253-64. doi: 10.1016/S0140-6736(13)61949-2.

[2] M. Lindenberg, S. Kopp, J.B. Dressman, Classification of orally administered drugs on the World Health Organization Model list of Essential Medicines according to the biopharmaceutics classification system. Eur J Pharm Biopharm 58 (2004) 265-278. doi: 10.1016/j.ejpb.2004.03.001

[3] N. Passerini, B. Albertini, B. Perissutti, L. Rodriguez, Evaluation of melt granulation and ultrasonic spray congealing as techniques to enhance the dissolution of praziquantel, Int J Pharm 318 (2006) 92-102. 10.1016/j.ijpharm.2006.03.028

[4] D.P. McManus, D.W. Dunne, M. Sacko, J. Utzinger, B.J. Vennervald, X.-N. Zhou, Schistosomiasis. Nat. Rev. Dis. Primers 4 (2018):13-. doi: 10.1038/s41572-018-0013-8

[5] D Cioli, L. Pica-Mattoccia, Praziquantel, Parasitol. Res. 90 Supp 1(2003) S3-9. doi: 10.1007/s00436-002-0751-z

[6] J.T. Coulibaly, G. Panic, K.D. Silue, J. Kovac, J. Hattendorf, J. Keiser. Efficacy and safety of praziquantel in preschool-aged and school-aged children infected with Schistosoma mansoni: a randomised controlled, parallel-group, dose-ranging, phase 2 trial, Lancet Glob Health. 5 (7) (2017) e688-e698. doi: 10.1016/S2214-109X(17)30187-0.

[7] D. Zanolla, B. Perissutti, N. Passerini, M.R. Chierotti, D. Hasa, D. Voinovich, L. Gigli, N. Demitri, S. Geremia, J. Keiser, P. Cerreia Vioglio, B. Albertini, A new soluble and bioactive polymorph of praziquantel, Eur J Pharm and Biopharm, 127 (2018) 19-28. doi: 10.1016/j.ejpb.2018.01.018

[8] C.R. Groom, I.J. Bruno, M.P. Lightfoot, S.C. Ward, The Cambridge Structural Database. Acta Crystallogr B Struct Sci Cryst Eng Mater 72 (2016)171-179. doi: 10.1107/S2052520616003954.

[9] F C. Lombardo, B.Perissutti, J. Keiser, Activity and pharmacokinetics of a praziquantel crystalline polymorph in the Schistosoma mansoni mouse model, submitted (20th February 2019).

[10] D. H. Doehlert, Uniform Shell Designs, Applied Statistics 19(3) (1970) 231-239. doi: 10.2307/2346327.

[11] G. Lewis, D. Mathieu, R. Phan-tan-luu, Pharmaceutical Experimental Design, CRC PRess, Marcel Dekker, New York, 1999, pp.221-235. doi:10.1201/9780203508688.

[12] T. Lundstedt, E. Seifert, L. Abramo, B. Thelin, A. Nyström, J. Pettersen, R. Bergman, Experimental design and optimization, Chemometrics and Intelligent Laboratory Systems 42 (1998), pp. 3–40. doi: 10.1016/S0169-7439(98)00065-3

[13] S.L.C Ferreira, W N L dos Santos, CM Quintella, BB Neto, JM Bosque-Sendra, Doehlert matrix: a chemometric tool for analytical chemistry—review, Talanta 63 (4) 2004, 1061-1067. doi: 10.1016/j.talanta.2004.01.015.

[14] S.L.C. Ferreira, R.E. Bruns, E.G.P. da Silva, W.N.L. dos Santos, C.M. Quintella, J.M. David, J.B. de Andrade, M.C. Breitkreitz, I.C.S.F. Jardim, B.B. Neto, Statistical designs and response surface techniques for the optimization of chromatographic systems, J Chrom A, 1158 (1-2) (2007) 2-14. DOI: 10.1016/j.chroma.2007.03.051

[15] M A Bezerra, R.E. Santelli, E.P. Oliveira, L.S. Villar, L.A. Escaleira, Response surface methodology (RSM) as a tool for optimization in analytical chemistry. TALANTA 76 (2008) 965-977. doi: 10.1016/j.talanta.2008.05.019. Epub 2008 May 21.

[16] D. Vojnovic, P. Rupena, M. Moneghini, F. Rubessa, S. Coslovich, R. Phan-Tan-Luu, R.M. Sergent, Experimental research methodology applied to wet pelletization in a high shear mixer. Part I, S.T.P., Pharma Sci. 3 (1993) 130–135.

[17] D. Vojnovic, D. Chicco, H. El Zenary, Doehlert experimental design applied to optimization and quality control of a granulation process in a high shear mixer, Int. J. Pharm. 145 (1996) 203-213. doi: 10.1016/S0378-5173(96)04771-0 10.1016/S0378-5173(96)04771-0

[18] D. Voinovich, M. Moneghini, B.Perissutti, J. Filipovic-Grcic, I. Grabnar, Preparation in high-shear mixer of sustained-release pellets by melt pelletisation, Int. J. Pharm. 203 (2000) 235. doi: 10.1016/S0378-5173(00)00455-5

[19] S. Thirunahari, P.S. Chow, R.B.H. Tan, Quality by design (QbD)-based crystallization process development for the polymorphic drug tolbutamide, Cryst Growth Des 11 (7) (2011), 3027-3038. doi: 10.1021/cg2003029

[20] D. Hasa, B. Perissutti, C. Cepek, S. Bhardwaj, E. Carlino, M. Grassi, S. Invernizzi, D. Voinovich, Drug salt formation via mechanochemistry: The case study of vincamine, Mol. Pharmaceutics, 10 (1) (2013), 211-224. DOI: 10.1021/mp300371f.

[21] K. Nagapudi, E.Y. Umanzor, C. Masui, High-throughput screening and scale-up of cocrystals using resonant acoustic mixing, Int J Pharm. 521 (1-2) (2017), 337-345. doi: 10.1016/j.ijpharm.2017.02.027

[22] A. De Gusseme, C Neves, JF Willart, A Rameau, M Descamps, Ordering and disordering of molecular solids upon mechanical milling: the case of fananserine, J Pharm. Sci. 97 (11) (2008) 5000-12. doi: 10.1002/jps.21472.

[23] J. C. Espinosa-Lara, D. Guzman-Villanueva, J. I. Arenas-García, D.Herrera-Ruiz, J. Rivera-Islas, P. Román-Bravo, H. Morales-Rojas, H. Höpfl, Cocrystals of Active Pharmaceutical Ingredients Praziquantel in Combination with Oxalic, Malonic, Succinic, Maleic, Fumaric, Glutaric, Adipic, And Pimelic Acids. Cryst. Growth Des. 13 (2013), 169−185. doi: 10.1021/cg301314w

[24] B. Perissutti, N. Passerini, R. Trastullo, J. Keiser, D. Zanolla, G. Zingone, D. Voinovich, B. Albertini, An explorative analysis of process and formulation variables affecting comilling in a vibrational mill: The case of praziquantel, Int J Pharm. 533 (2) (2017) 402-412. doi: 10.1016/j.ijpharm.2017.05.053

[25] D. Mathieu, J. Nony, R. Phan-Tan-Luu, New Efficient Technology for Research using Optimal Desing (NEMRODW), software L.P.R.A.I., Marseille (2011).

[26] Y. Sun, S. J. Bu, Simple, cheap and effective high-performance liquid chromatographic method for determination of praziquantel in bovine muscle, J. Chromatogr. B 899 (2012), 160–162. doi: 10.1016/j.jchromb.2012.05.004

[27] A. Cedillo-Cruz, M. I. Aguilar, M. Flores-Alamo, F. Palomares-Alonso, H. Jung-Cook, A straightforward and efficient synthesis of praziquantel enantiomers and their 40-hydroxy derivatives. Tetrahedron: Asymmetry 25 (2014), 133–140.

[28] P. Roszkowski, J. K. Maurin, Z. Czarnocki, Enantioselective synthesis of (R)-(−)-praziquantel (PZQ), Tetrahedron: Asymmetry 17 (9) (2006), 1415-1419. doi: 10.1016/j.tetasy.2006.04.023

[29] A. Lausi, M. Polentarutti, S. Onesti, J. R. Plaisier, E. Busetto, G. Bais, L. Barba, A. Cassetta, G. Campi, D. Lamba, A. Pifferi, S.C. Mande, D.D. Sarma, S.M. Sharma, G. Paolucci, Status of the crystallography beamlines at Elettra, The European Physical Journal Plus, 130 (3) (2015), 1-8. doi: 10.1140/epjp/i2015-15043-3.

[30] A.P. Hammersley, S.O. Svensson, M. Hanfland, A. N. Fitch, and D. Häusermann, Two-Dimensional Detector Software: From Real Detector to Idealised Image or Two-Theta Scan, High Pressure Research 14 (1996) 235-248. doi: 10.1080/08957959608201408

[31] A P. Hammersley, ESRF Internal Report, ESRF98HA01T, FIT2D V9.129 Reference Manual V3.1 (1998)

[32] S. J. Clark, M. D. Segall, C. J. Pickard, P. J. Hasnip, M. J Probert, K.Refson, M. C. Payne, First principles methods using CASTEP, Z. Kristallogr. 220 (2005), 567–570. doi: 10.1524/zkri.220.5.567.65075

[33] P. J. Hasnip, K. Refson, M. I. J. Probert, J. R. Yates, S. J. Clark, C. J. Pickard, Density functional theory in the solid state, Philos. Trans. R. Soc. A-Math. Phys. Eng. Sci. 372 (2014) 20130270. doi: 10.1098/rsta.2013.0270

[34] C. J. Pickard and F.Mauri, All-electron magnetic response with pseudopotentials: NMR chemical shifts, Phys. Rev. B 63 (2001), 245101. doi: 10.1103/PhysRevB.63.245101

[35] J. P. Perdew, K. Burke, M. Ernzerhof, Generalized Gradient Approximation Made Simple, Phys. Rev. Lett. 1996, 77, 3865–3868. Erratum Phys. Rev. Lett. 78, 1396 (1997) doi: 10.1103/PhysRevLett.77.3865.

[36] E. R. McNellis, J. Meyer and K. Reuter, Azobenzene at coinage metal surfaces: Role of dispersive van der Waals interactions, Phys. Rev. B, 80 (2009), 205414. doi: 10.1103/PhysRevB.80.205414

[37] A. Tkatchenko and M. Scheffler, Accurate Molecular Van Der Waals Interactions from Ground-State Electron Density and Free-Atom Reference Data, Phys. Rev. Lett. 102 (2009) 73005. doi: 10.1103/PhysRevLett.102.073005

[38] R. K. Harris, P. Hodgkinson, C. J. Pickard, J. R. Yates, V. Zorin, Chemical shift computations on a crystallographic basis: some reflections and comments, Magn. Reson. Chem., 45 (2007), S174–S186. doi: 10.1002/mrc.2132.

[39] G.N.M. Reddy, D. S. Cook, D. Iuga, R.I. Walton, A. Marsh, S.P. Brown, Co-existence of Distinct Supramolecular Assemblies in Solution and in the Solid State, Solid State Nucl. Magn. Reson., 65 (2015) 41–48. doi: 10.1002/chem.201604832

[40] F C. Lombardo, V Pasche, G Panic, Y Endriss, J. Keiser, Life cycle maintenance and drug-sensitivity assays for early drug discovery in Schistosoma mansoni, Nature Protocols 14 (2019) 461–481. doi: 10.1038/s41596-018-0101-y

[41] S. L. James, C.J. Adams, C. Bolm, D. Braga, P Collier, T Friščić, F Grepioni, K. D. M. Harris, G. Hyett, W. Jones, A Krebs, J Mack, L Maini, A. Guy Orpen, I P. Parkin, W. C. Shearouse, J W. Steedk, D. C. Waddelli, Mechanochemistry: opportunities for new and cleaner synthesis, Chem. Soc. Rev. 41 (2012), 413–447. doi: 10.1039/c1cs15171a

[42] W. Jones and M.D.Eddleston, Introductory lecture: Mechanochemistry, a versatile synthesis strategy for new materials. Faraday Discuss. 170 (2014), 9-34. doi:10.1039/C4FD00162A

[43] A.M. Belenguer, G.I. Lampronti, J. K M.. Sander, Reliable Mechanochemistry: Protocols for Reproducible Outcomes of Neat and Liquid Assisted Ball-mill Grinding Experiments. J. Vis. Exp. 131 (2018), e56824, doi:10.3791/56824

[44] I. A. Tumanov, A. A. L. Michalchuk, A.A. Politov, E.V. Boldyreva, V.V. Boldyrev, Inadvertent liquid assisted grinding: a key to “dry” organic mechano-co-crystallisation? CrystEngComm, 19 (2017) 2830-2835. doi: 10.1039/C7CE00517B (Communication).

[45] Biltricide data sheet. url: https://www.accessdata.fda.gov/drugsatfda_docs/label/2014/018714s013lbl.pdf.

[46] D. Hasa, D. Voinovich, B. Perissutti, G. Grassi, S. Fiorentino, R. Farra, M. Abrami, I. Colombo, M. Grassi, Reduction of melting temperature and enthalpy of drug crystals: Theoretical aspects, Eur J Pharm Sci 50.1 (2013), 17–28. DOI: 10.1016/j.ejps.2013.03.018

[47] D. Zanolla, B. Perissutti, N. Passerini, S. Invernizzi, D. Voinovich, S. Bertoni, C. Melegari, G. Millotti, B. Albertini, Milling and comilling Praziquantel at cryogenic and room temperatures: Assessment of the process-induced effects on drug properties, J Pharm Biomed Anal. 153(2018), 82-89. 10.1016/j.jpba.2018.02.018

[48] N. Chieng, Z. Zujovic, G. Bowmaker, T. Rades, D. Saville, Effect of milling on the solid-state conversion of ranitidine hydrochloride form 1, Int. J. Pharm. 327 (2006) 36-44. doi: 10.1016/j.ijpharm.2006.07.032

[49] M. Descamps, J.F. Willart, E. Dudognon, V. Caron, Transformation of pharmaceutical compounds upon milling and comilling: The role of Tg, J. Pharm. Sci. 96 (5) (2007) 1398–1407. doi: 10.1002/jps.20939.

[50] B. Schammé, X. Monnier, N. Couvrat, L. Delbreilh, V. Dupray, E. Dargent, G. Coquerel, Insights on the Physical State Reached by an Active Pharmaceutical Ingredient upon High-Energy Milling, J. Phys. Chem. B 121 (2017), 5142−5150. doi: 10.1021/acs.jpcb.7b02247.

[51] I. Šagud, D. Zanolla, B. Perissutti, N. Passerini, I. Škorić, Identification of degradation products of praziquantel during the mechanochemical activation, J Pharm Biomed Anal. 159 (2018), 291-295. DOI: 10.1016/j.jpba.2018.07.002

[52] A.Altomare, C. Cuocci, C.Giacovazzo, A.Moliterni, R. Rizzi, N.Corriero, A. Falcicchio, EXPO2014. A kit of tools for phasing crystal structures solution by powder diffraction data, J. Appl. Cryst. 46 (2013), 1231-1235. doi:10.1107/S0021889813013113

[53] A. L. Spek, Structure validation in chemical crystallography. Acta Cryst. D65 (2) (2009), 148-155. doi: 10.1107/S090744490804362X

[54] F. Macrae, I. J. Bruno, J. A. Chisholm, P.R. Edgington, P. McCabe, E. Pidcock, L. Rodriguez-Monge, R. Taylor, J. van de Streek, P.A. Wood, Mercury CSD 2.0 - New Features for the Visualization and Investigation of Crystal Structures, J. Appl. Cryst., 41 (2008), 466-470. doi: 10.1107/S0021889807067908

[55] P. Cerreia Vioglio, L. Catalano, V. Vasylyeva, C.Nervi, M.R. Chierotti, G. Resnati, R. Gobetto, P. Metrangolo, Natural Abundance ^{15}N and ^{13}C Solid-State NMR Chemical Shifts: High Sensitivity Probes of the Halogen Bond Geometry, Chemistry 22 (47) (2016), 16819-16828. doi: 10.1002/chem.201603392

[56] S.D. Gumbert, M. Körbitzer, E. Alig, E., M.U. Schmidt, M.R. Chierotti, R. Gobetto, X. Li, J. Van De Streek, Crystal structure and tautomerism of Pigment Yellow 138 determined by X-ray powder

diffraction and solid-state NMR, Dyes and Pigments 131(2016) 364-372. doi: 10.1016/j.dyepig.2016.03.035

[57] F. Rossi, P. Cerreia Vioglio, S. Bordignon, V. Giorgio, C. Nervi, E. Priola, R. Gobetto, K. Yazawa, M.R. Chierotti, Unraveling the Hydrogen Bond Network in a Theophylline-Pyridoxine Salt Cocrystal by a Combined X-ray Diffraction, Solid-State NMR, and Computational Approach, Cryst. Growth Des. 18 (4) (2018), 2225-2233. doi:: 10.1021/acs.cgd.7b01662

[58] J.D. Hartman, R.A. Kudla, G.M. Day, L.J. Mueller, G.J.O. Beran, Benchmark fragment-based 1H, 13C, 15N and 17O chemical shift predictions in molecular crystals, Phys Chem Chem Phys. 18(31) (2016) 21686–21709. doi: 10.1039/c6cp01831a

[59] A. Borrego-Sánchez, C. Viseras, C. Aguzzi, C.I. Sainz-Díaz, Molecular and crystal structure of praziquantel. Spectroscopic properties and crystal polymorphism. Eur J Pharm Sci 92 (2016), 266–275. Doi: 10.1016/j.ejps.2016.04.023

[60] E.C. Arrúa,, M.J.G. Ferreira, C.J. Salomon, T.G. Nunes, Elucidating the guest-host interactions and complex formation of praziquantel and cyclodextrin derivatives by 13C and 15N solid-state NMR spectroscopy, Int J Pharm 496 (2015) 812–821. doi: 10.1016/j.ijpharm.2015.11.026

[61] T. P. Shakhtshneider, Phase transformations and stabilization of metastable states of molecular crystals under mechanical activation, Solid State Ionics 101–103 (1997), 851–856. doi: 10.1016/S0167-2738(97)00224-5

[62] G. Mayoka, J. Keiser , G. Haeberli, K.Chibale, Structure−Activity Relationship and in Vitro Absorption, Distribution, Metabolism, Excretion, and Toxicity (ADMET) Studies of N□aryl 3□Trifluoromethyl Pyrido[1,2□a]benzimidazoles That Are Efficacious in a Mouse Model of Schistosomiasis, ACS Infect Dis. 2018 Dec 23. doi: 10.1021/acsinfecdis.8b00313.

[63] W. Ostwald, Studien uber die Bildung und umwandlung fester Korper, Zeitschrift fur Physic. 22 (1897), 289-330.

Figure legends

Figure 1. Chemical structure of Praziquantel (PZQ) with atom numbering.

Figure 2. Distribution of the experiments in the rotated Doehlert design for two variables and different PZQ crystal forms otbatined in each experimental point (y1): Blue circles indicate Praziquantel Form B, Red circles Form C; ligth (blue and red) colors indicate a reduced crystallinity degree of Form B and C, respectively; Green cyrcles designate miscellaneaus of solid forms (mixture of amorphous and other crystal forms).

Figure 3 XRPD diffractograms representing the 3 solid states (y1) found in the design space compared to commercial PZQ; arrows highlight peculiar signals of each solid form.

Figure 4. Temperature inside the jars during grinding at different frequencies measured using thermojars (according to paragraph. 2.2.1.).

Figure 5. d(0.5) values and error bars (n=3) for the 10 ground samples (x axis reports the numbers of the experimental trial, blue circles indicate PZQ Form B, red circles Form C and green cyrcles designate mixture of solid forms (mixture of amorphous and other crystal forms).

Figure 6. DSC traces of Form C (red), B (blue) and commercial PZQ (black).

Figure 7. ESEM images of Form C (EXP 10) [magnification 50X, 250 x, 500x, 1000x] compared to Scanning Electron Micrographs of Form B (EXP 7) [mag. 80x, 2200x in the frame] and commercial PZQ [mag. 151x, 2200x in the frame].

Figure 8. Rietveld refinement profile fit of Form C: in black the experimental pattern (collected using synchrotron radiation 0.700 Å), in red the calculated one. Residuals are displayed in blue and reflection ticks Atom: C 17 have been simulated from structure solution, and are reported in green.

Figure 9. Capped stick representation of the proposed strucure and crystal packing for Form C racemic mixture. The monoclinic centrosymmetric unit cell hosts 8 molecules, one crystallographically independent, in a I2/c space group.

Figure 10. (top) ^{13}C (100.65 MHz) CPMAS spectra with principal group assignments of commercial PZQ (a) Form B (b), Form C (c) recorded at 12 kHz; (bottom) ^{15}N (40.55 MHz) spectra of commercial PZQ (a) Form B (b), Form C (c) recorded at 9 KHz.

Figure 11. Overlay of the crystal structure of the polymorph C of PZQ from XRPD data and its geometry-optimized crystal structure by DFT calculations (in green). An all-atom root-mean-square value of 0.176 Å was obtained by the comparison of the two crystal structures, using the software Mercury (CCDC, v3.10) (Macrae et al., 2008). The positions of the hydrogen atoms were ignored.

Figure 12. Comparison of the XRPD patterns of Form C crystal structure: in black, the simulation obtained from the DFT-optimized structure; in red, the simulated powder diffractogram of the Form C using the experimental crystal structure. Both simulations were carried out with Mercury by setting a wavelength of 0.700Å.

Figure 13. Plot of the GIPAW-calculated 13C isotropic chemical shifts against the experimental 13C isotropic chemical shifts. The line of best fit is δiso(calc) = 1.02[δiso(exp)] – 1.80, and the Pearson's correlation coefficient is 0.9996.

Figure 14. FT-IR spectra of the three PZQ polymorphic varieties

Figure 15. Water solubility at 20°C of the anhydrous forms of PZQ.

Figure 16. DSC curves of Form C on aging. From top to down: Fresh sample and samples after 1, 2, 3, 4 months.

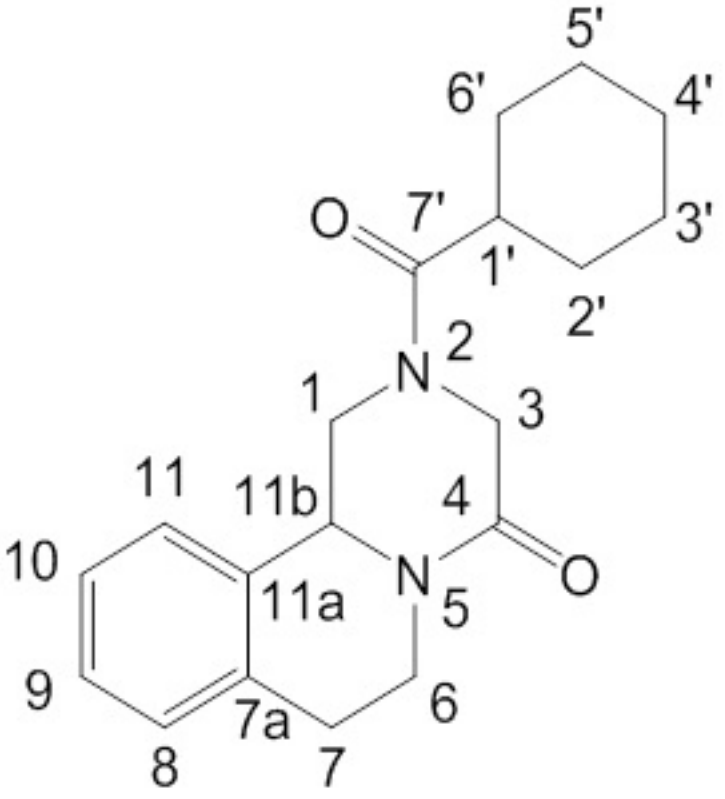
5'
6'
4'
O
7'
3'
1'
2'
N
2
1
3
11
11b
4
10
N
O
11a
5
9
6
7a
8
7

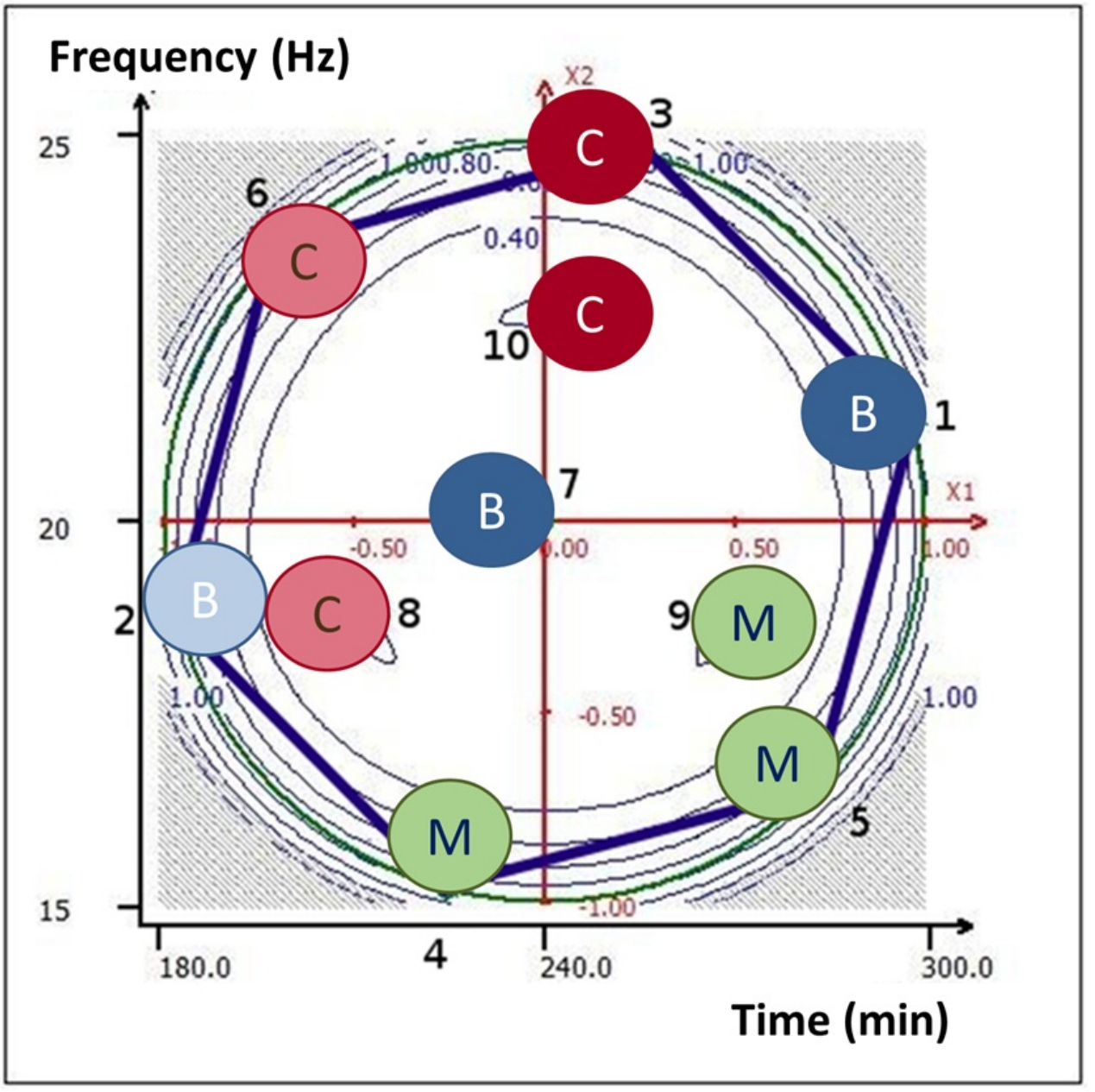
Frequency (Hz)
25
20
15
X2
X1
C
3
6
C
C
10
B
1
B
7
B
2
C
8
9
M
M
M
5
4
1.00
0.80
0.40
-0.50
0.00
0.50
1.00
-0.50
-1.00
180.0
240.0
300.0
Time (min)

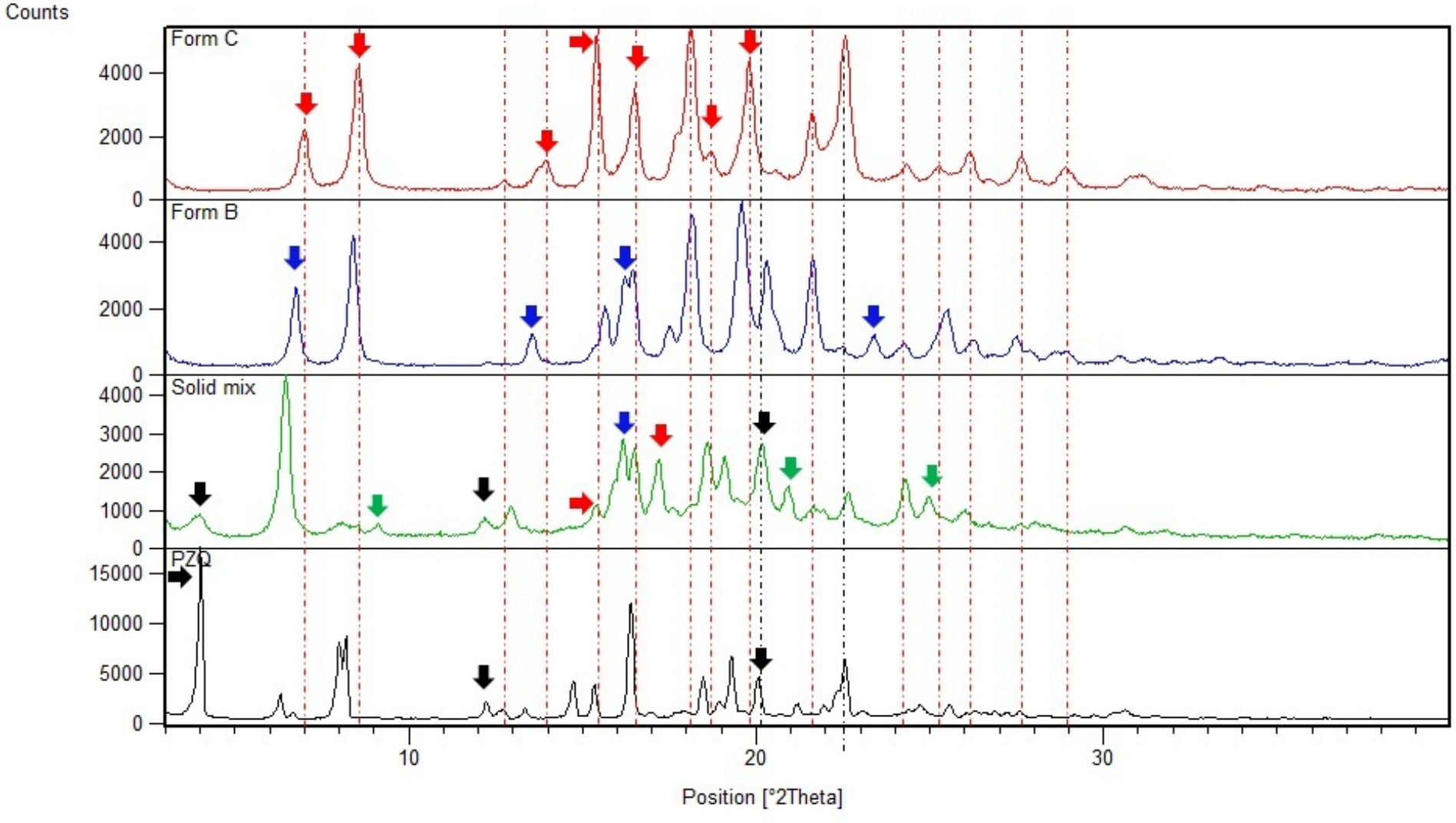
Counts
Form C
4000
2000
0
Form B
4000
2000
0
Solid mix
4000
3000
2000
1000
0
PZQ
15000
10000
5000
0
10
20
30
Position [°2Theta]

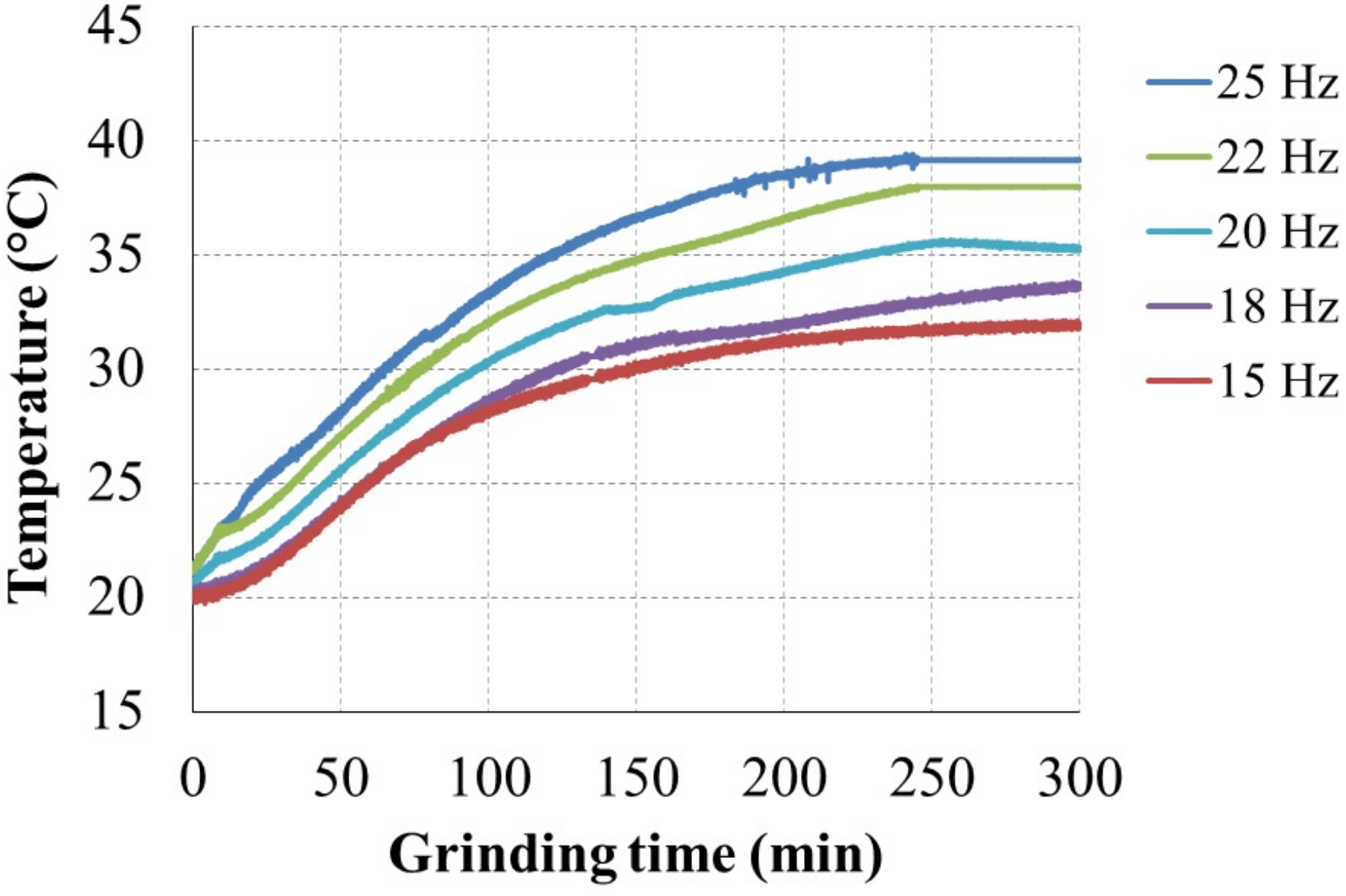
45
40
35
30
25
20
15
Temperature (°C)
0
50
100
150
200
250
300
Grinding time (min)
25 Hz
22 Hz
20 Hz
18 Hz
15 Hz

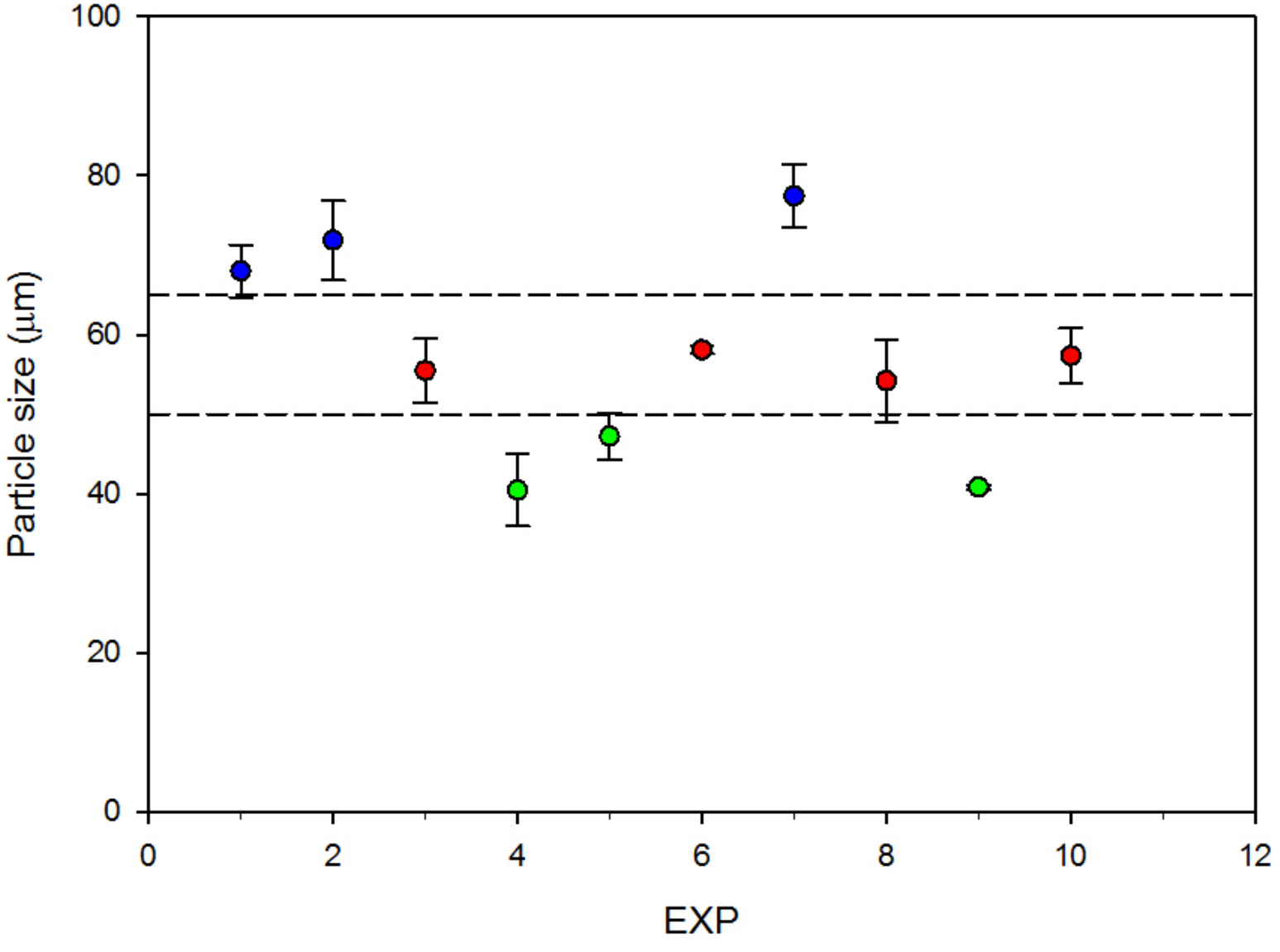
100
80
60
40
20
0
Particle size (µm)
0
2
4
6
8
10
12
EXP

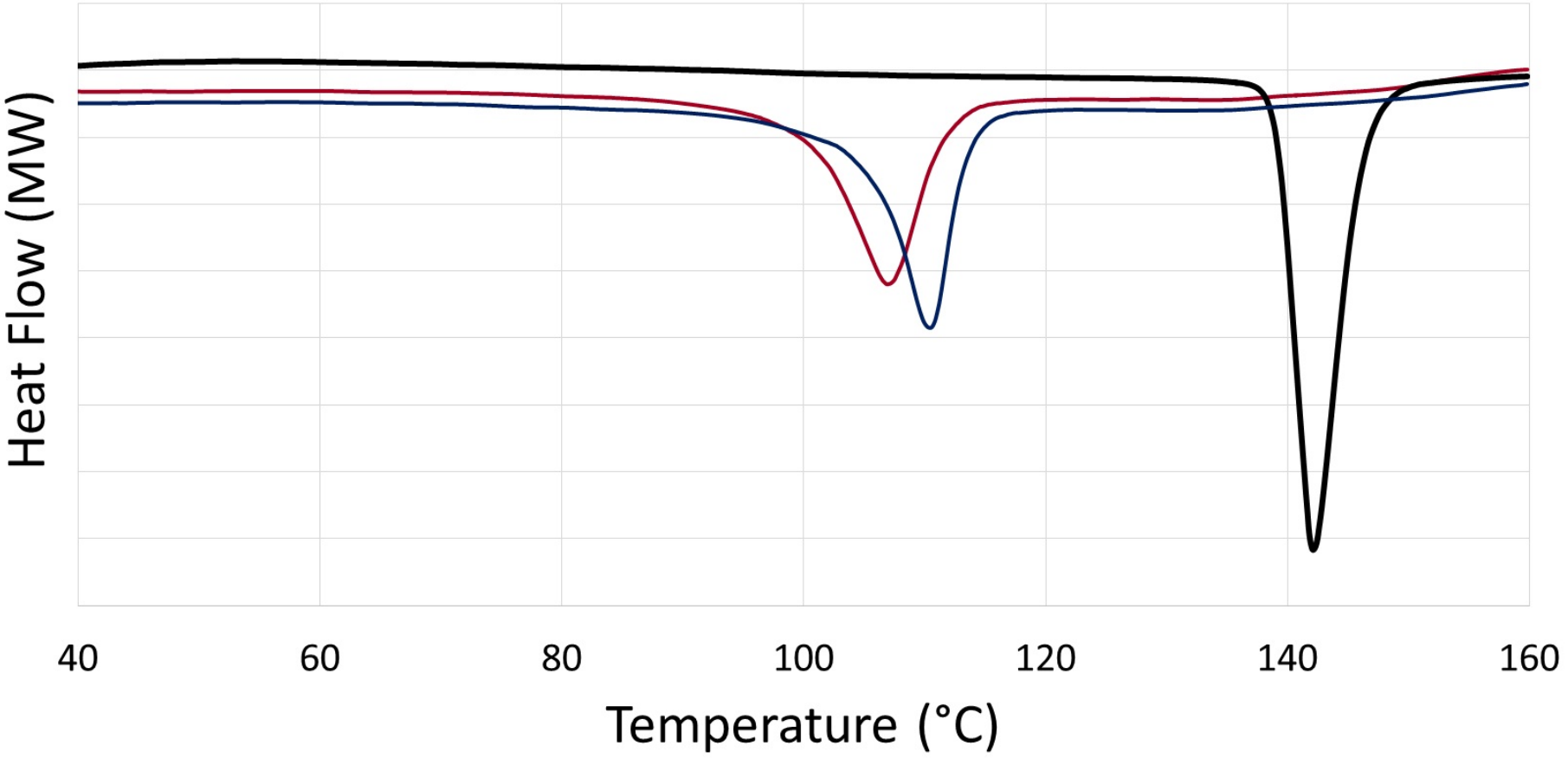
Heat Flow (MW)
40
60
80
100
120
140
160
Temperature (°C)

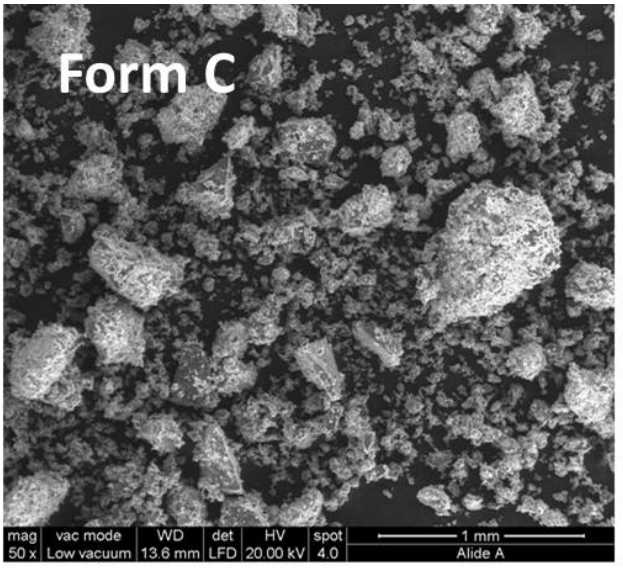
Form C
mag vac mode WD det HV spot
50 x Low vacuum 13.6 mm LFD 20.00 kV 4.0
1 mm
Alide A

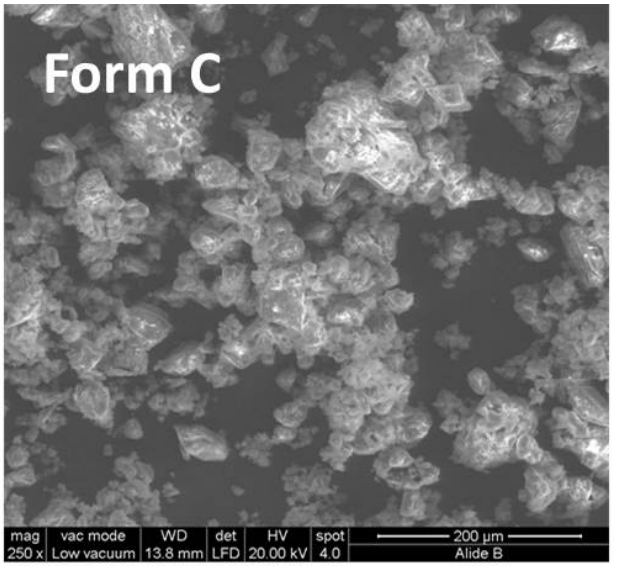
Form C
mag vac mode WD det HV spot
250 x Low vacuum 13.8 mm LFD 20.00 kV 4.0
200 µm
Alide B

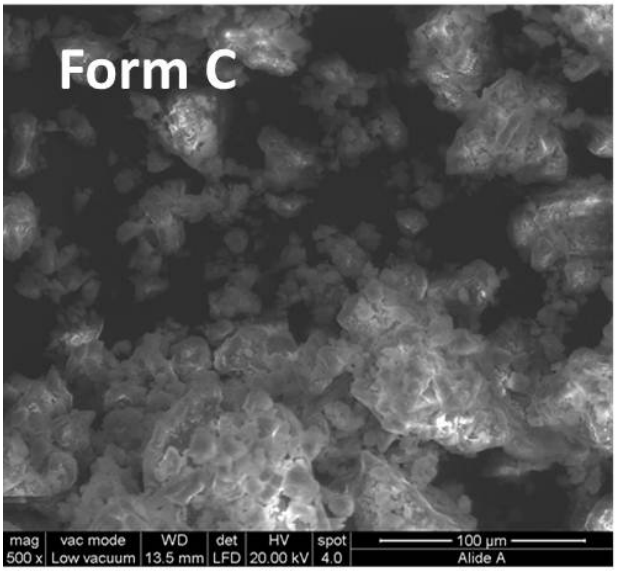
Form C
mag vac mode WD det HV spot
500 x Low vacuum 13.5 mm LFD 20.00 kV 4.0
100 µm
Alide A

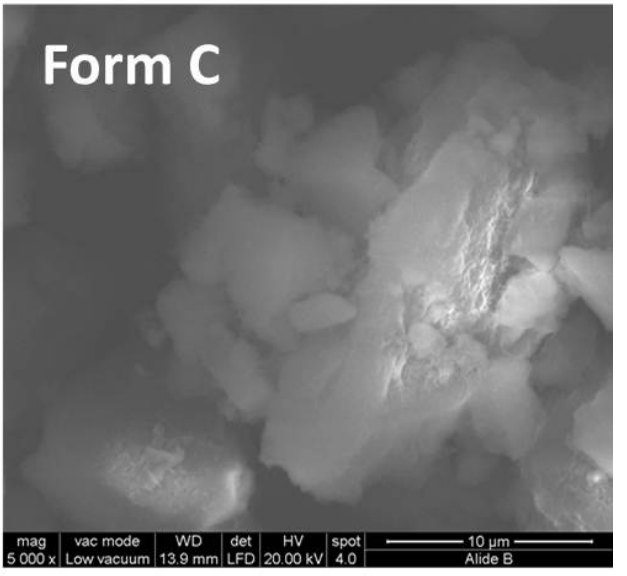
Form C
mag vac mode WD det HV spot
5 000 x Low vacuum 13.9 mm LFD 20.00 kV 4.0
10 µm
Alide B

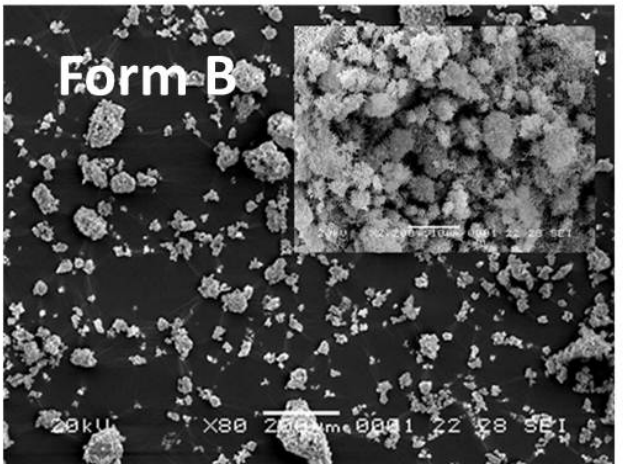
Form B

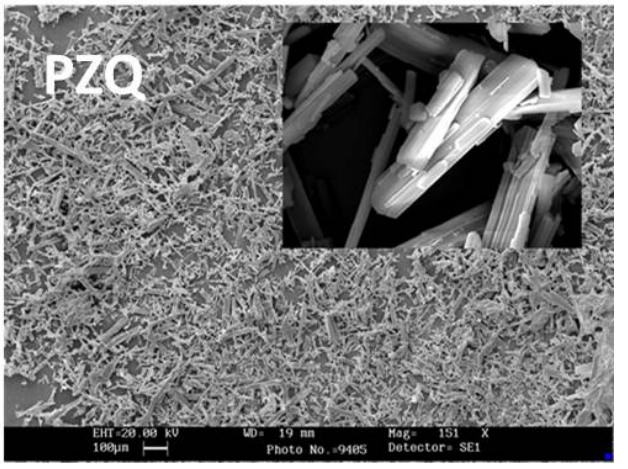
PZQ
EHT=20.00 kV
WD= 19 mm
Mag= 151 X
100µm
Photo No.=9405
Detector= SE1

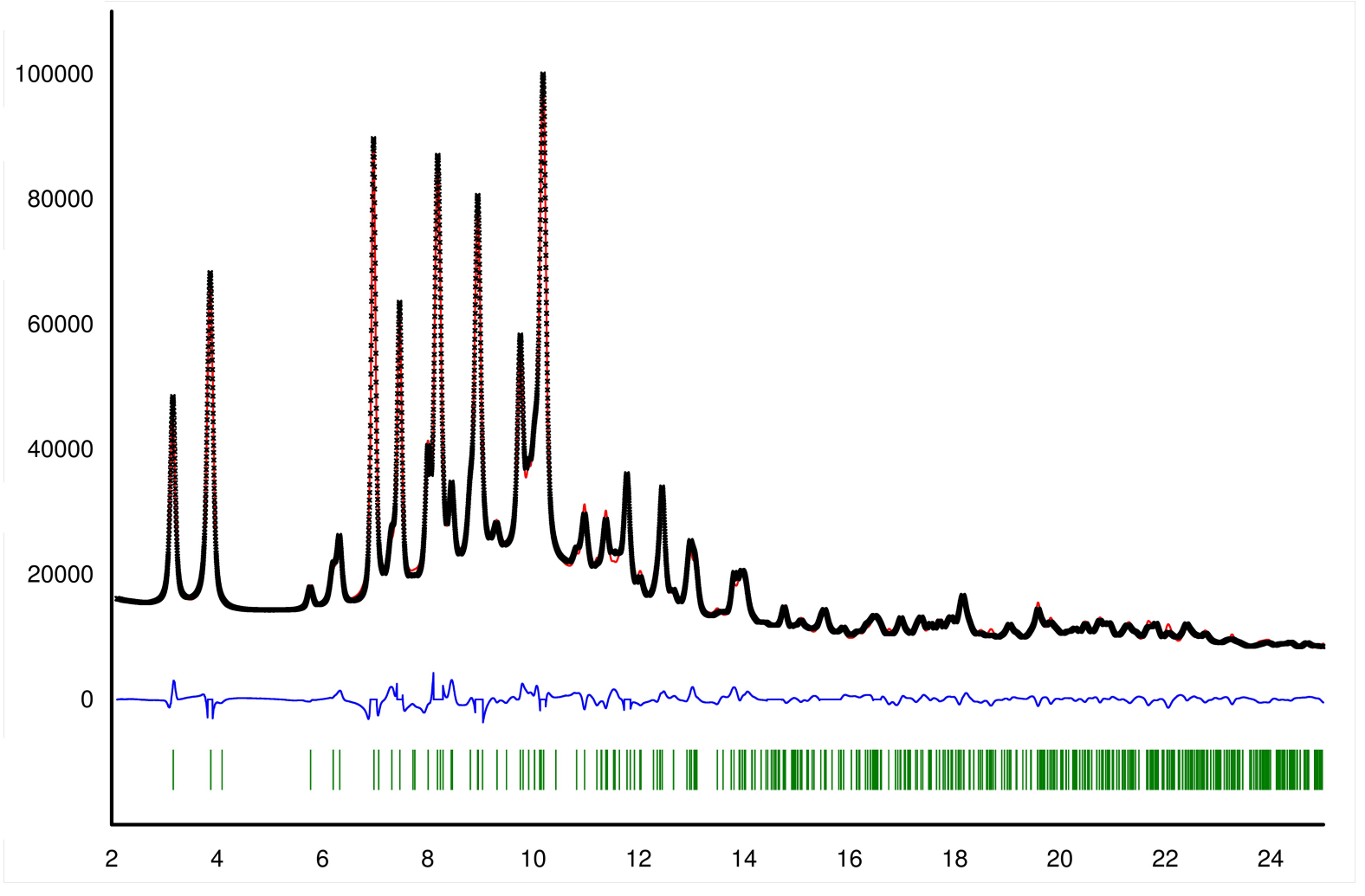
100000
80000
60000
40000
20000
0
2
4
6
8
10
12
14
16
18
20
22
24

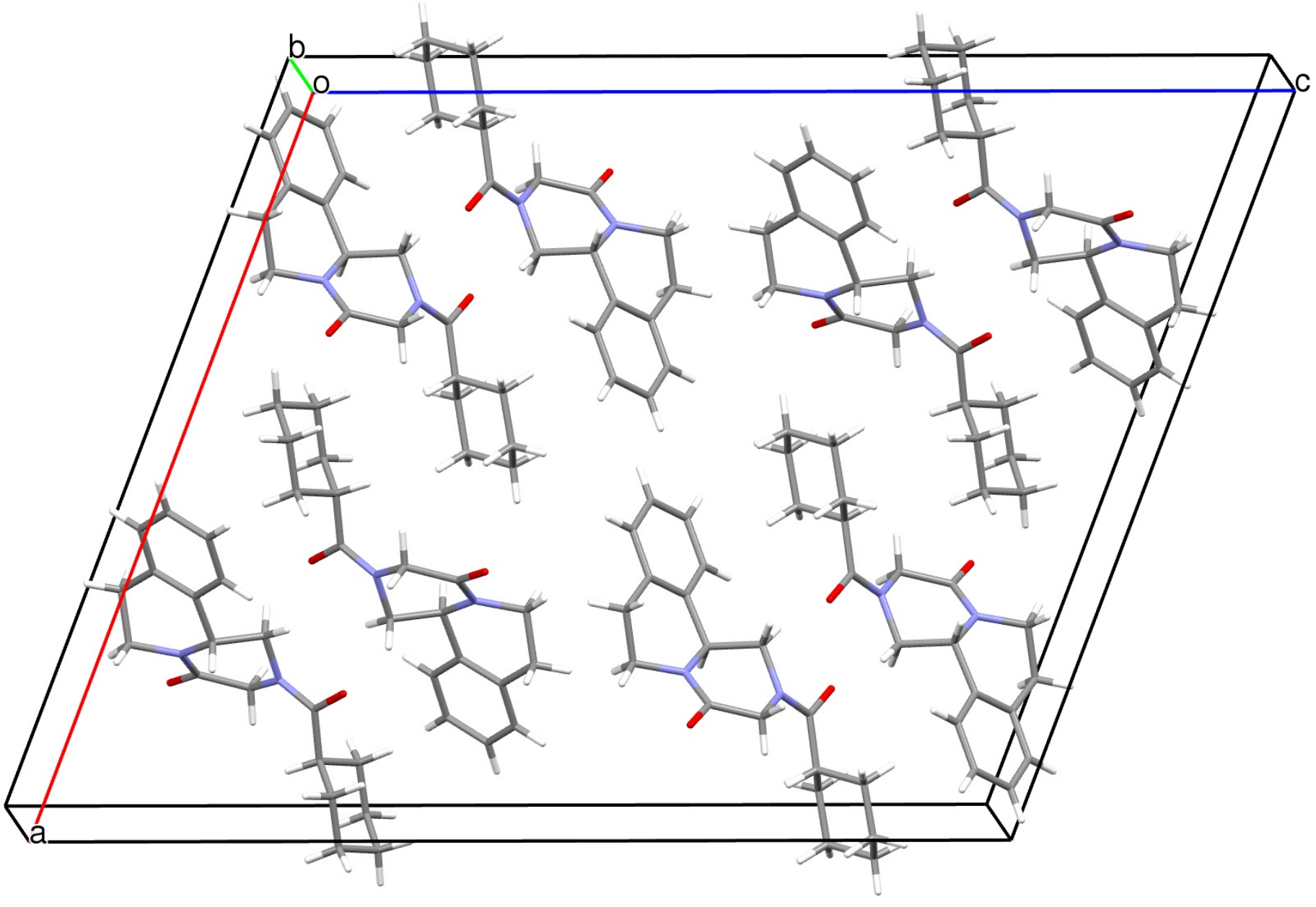
b
o
c
a

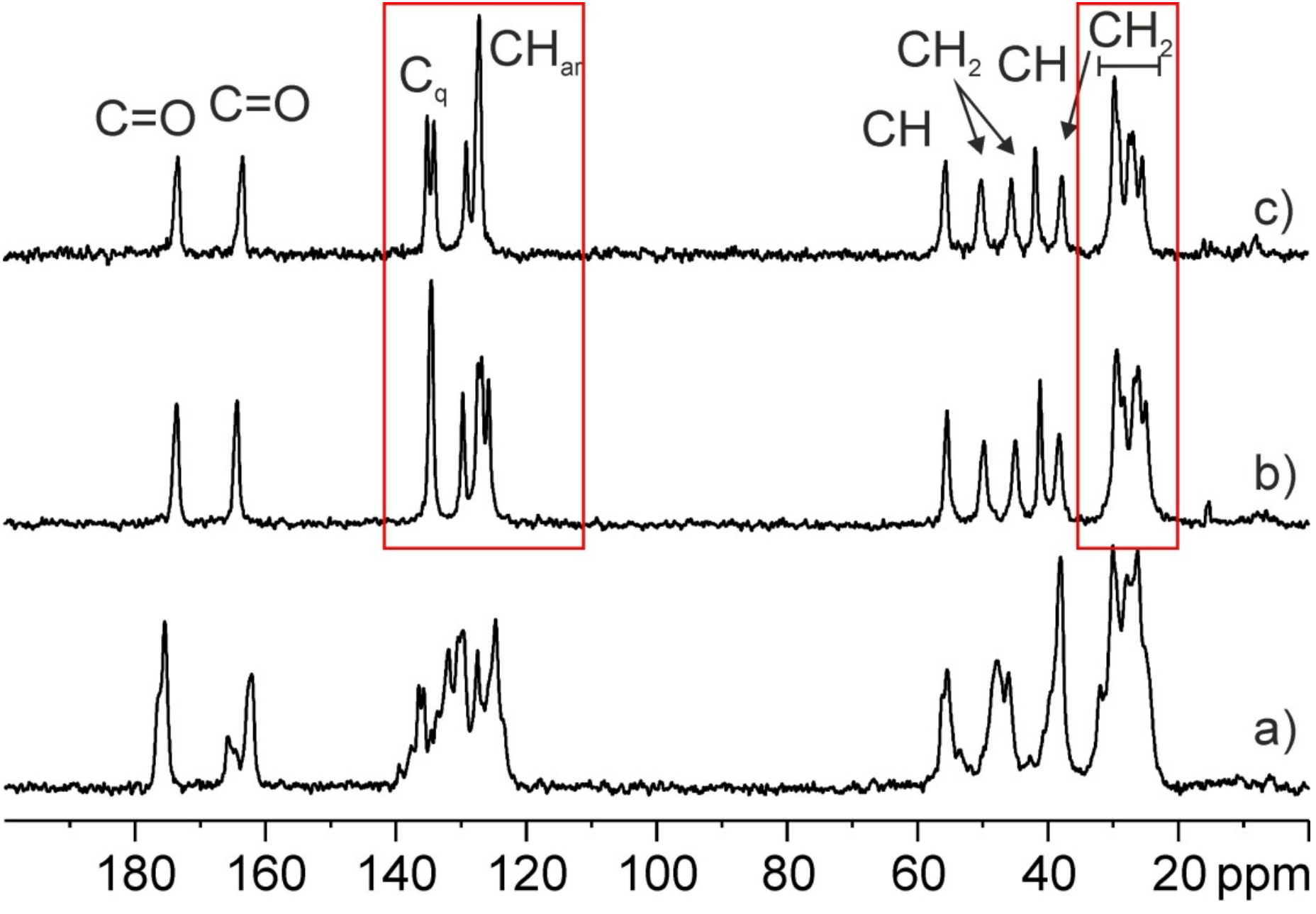
C=O
C=O
C$_q$
CH$_{ar}$
CH
CH$_2$
CH
CH$_2$
c)
b)
a)
180
160
140
120
100
80
60
40
20
ppm

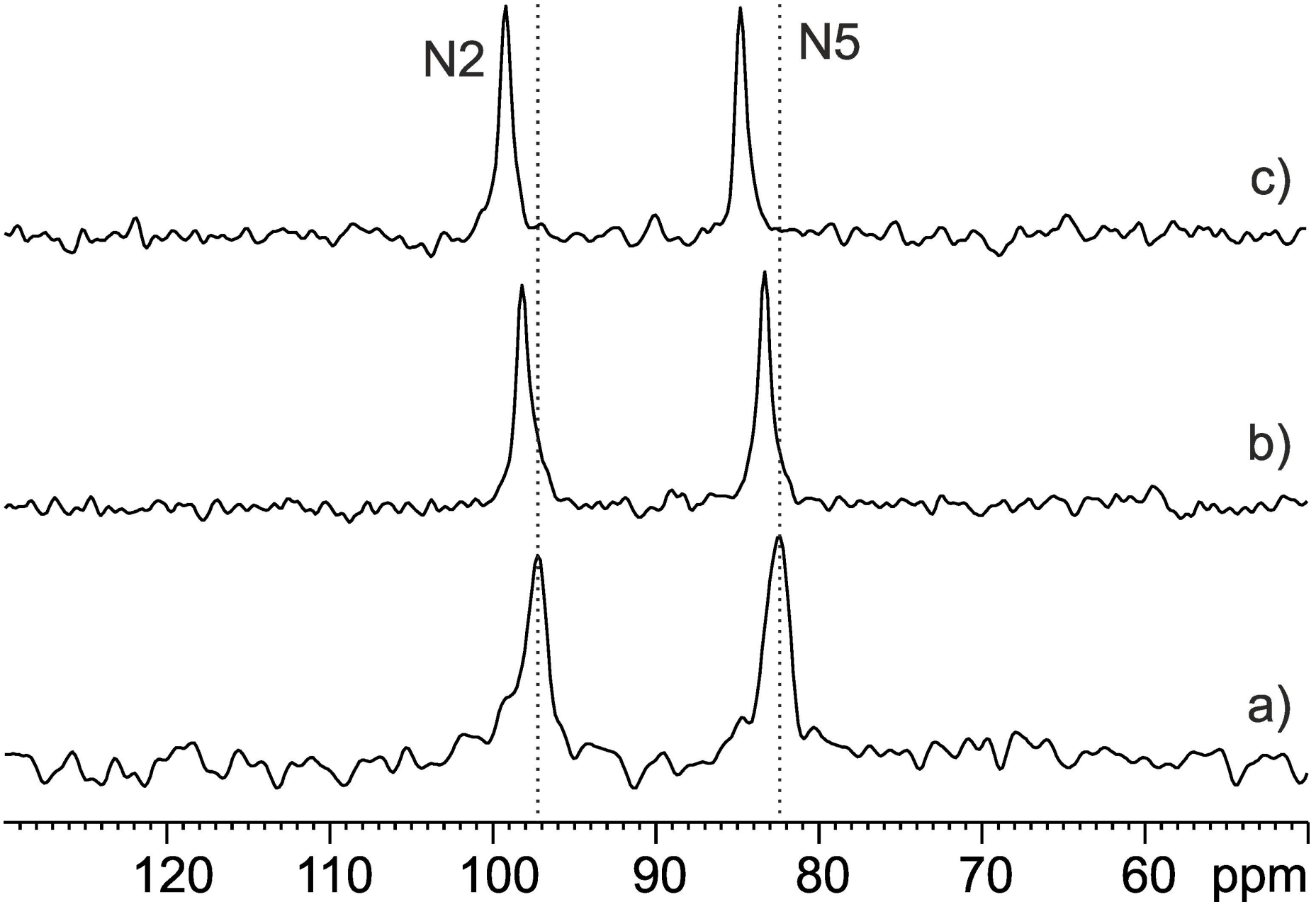
N2
N5
c)
b)
a)
120
110
100
90
80
70
60
ppm

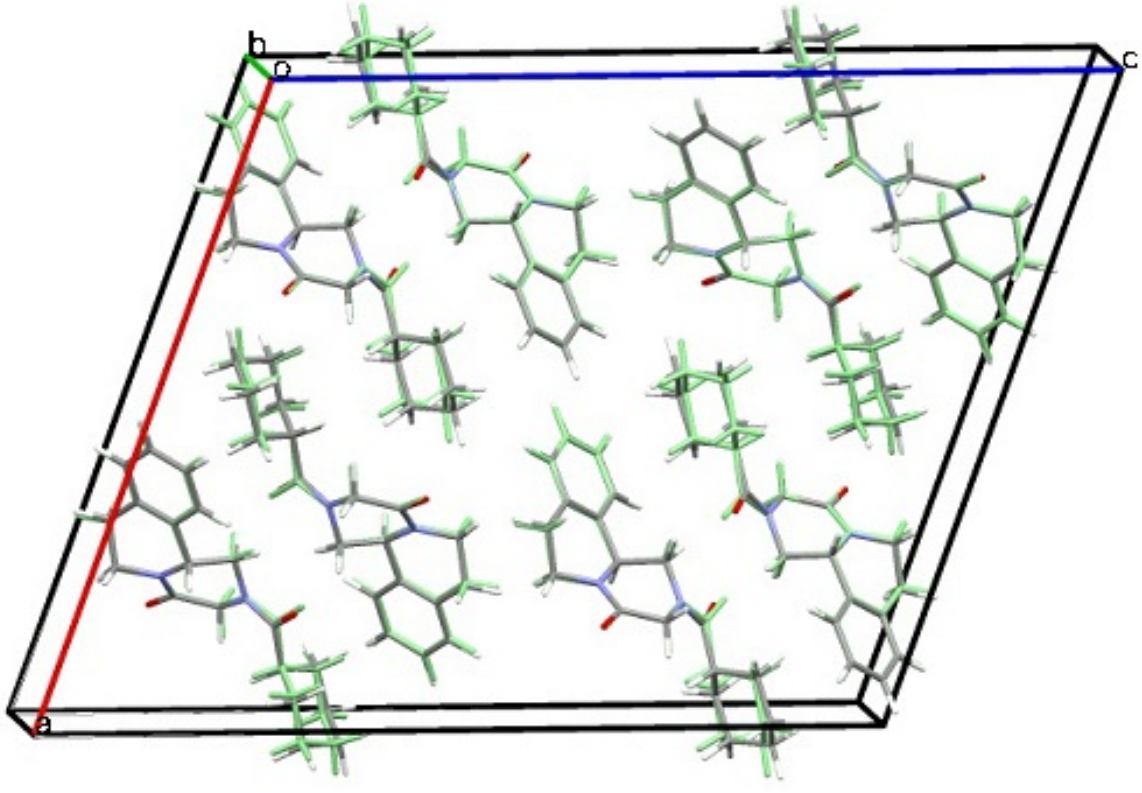
b
o
c
a

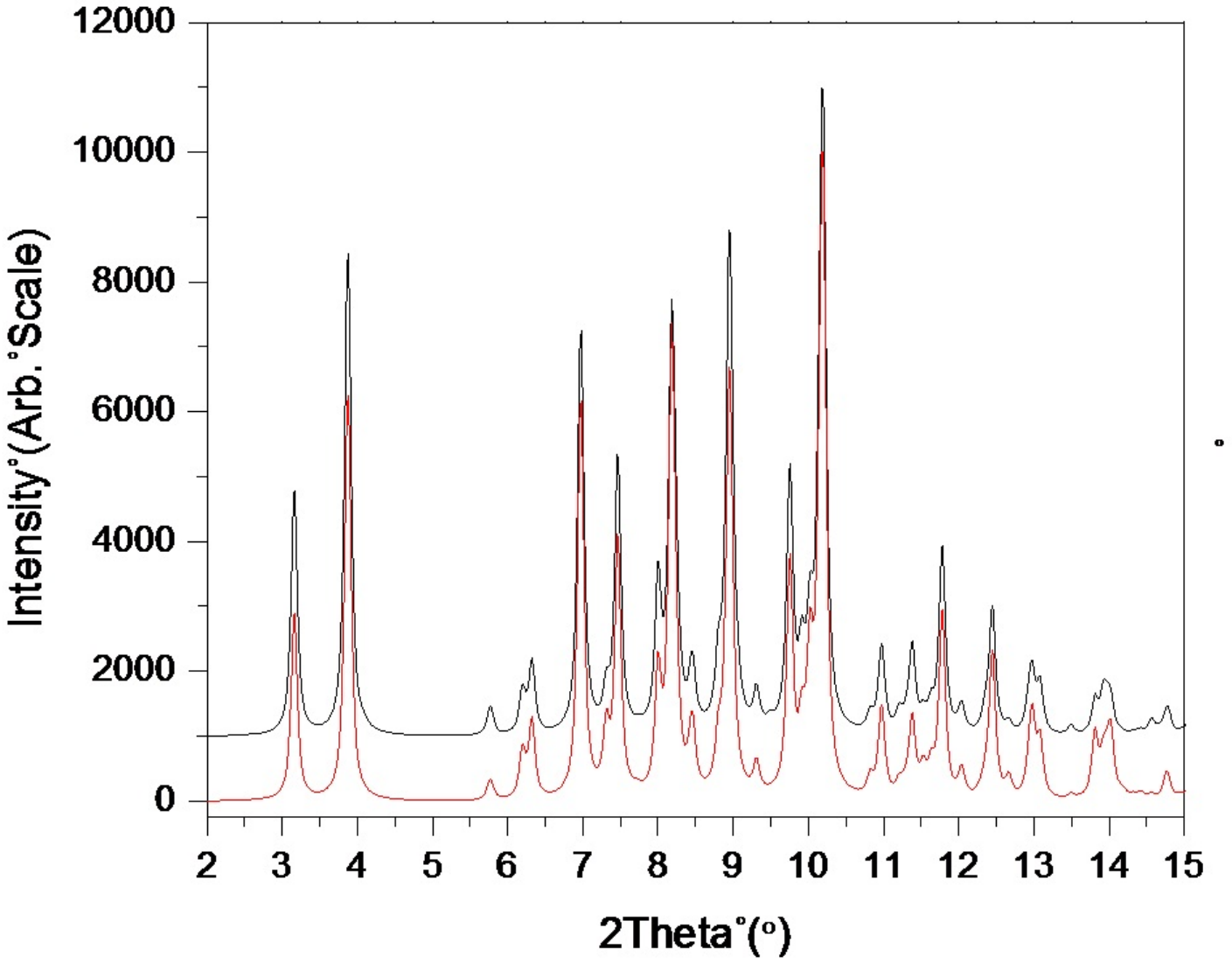
12000
10000
8000
6000
4000
2000
0
Intensity (Arb. Scale)
2
3
4
5
6
7
8
9
10
11
12
13
14
15
2Theta (°)

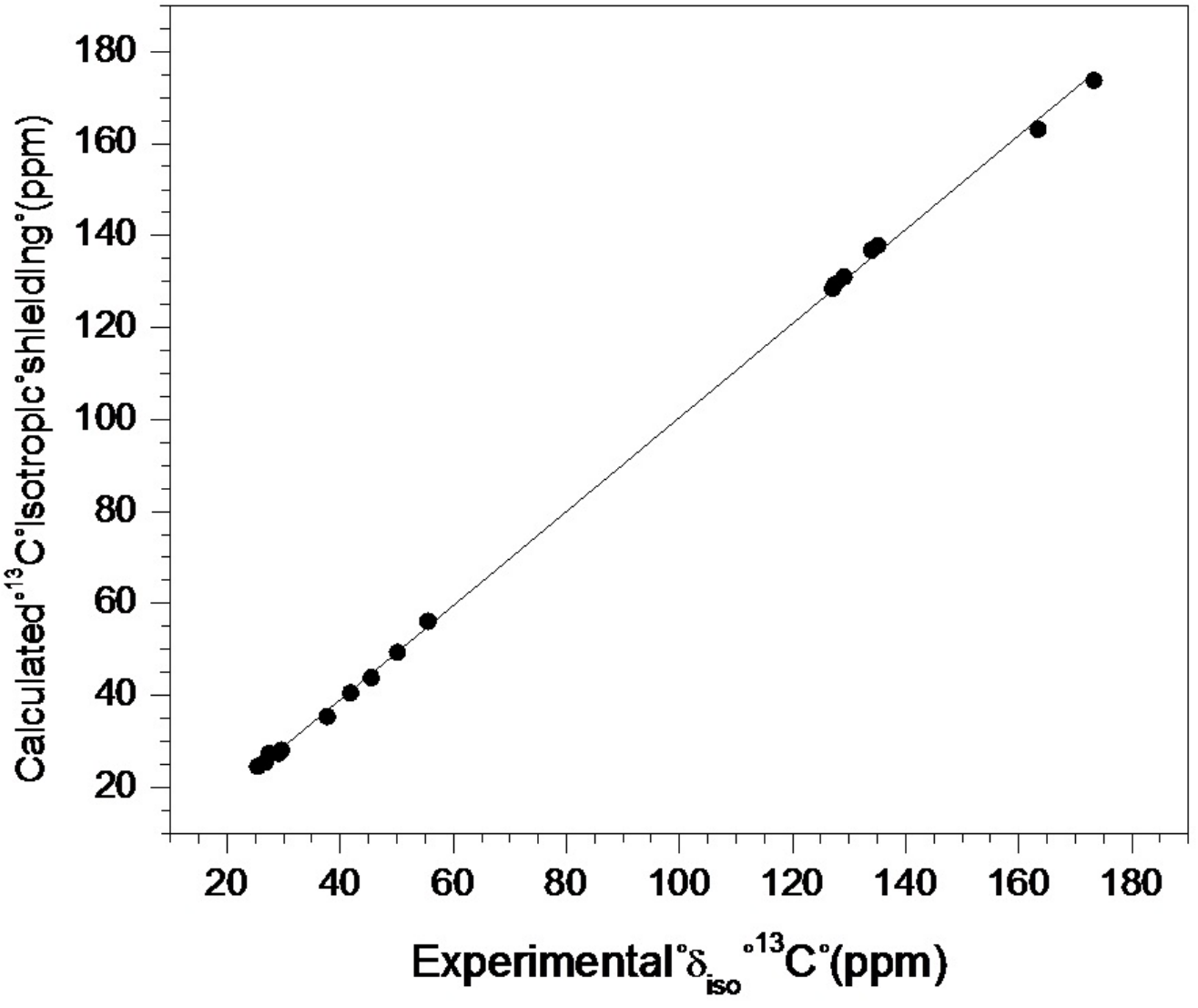
Calculated °13C°Isotroplc°shleldlng°(ppm)
Experimental °δiso °13C°(ppm)
20
40
60
80
100
120
140
160
180

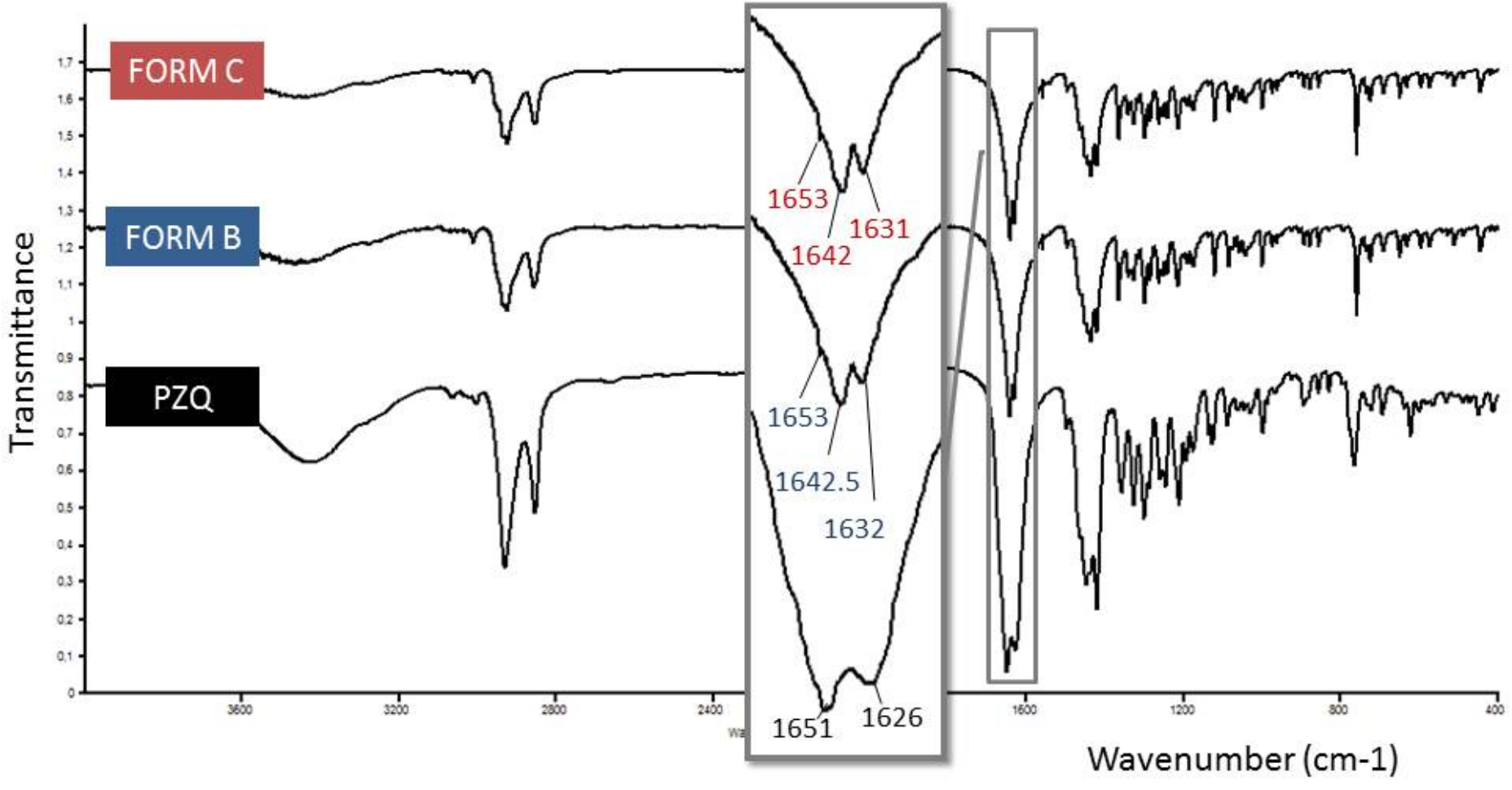
FORM C
FORM B
PZQ
Transmittance
Wavenumber (cm-1)
1653
1631
1642
1653
1642.5
1632
1651
1626

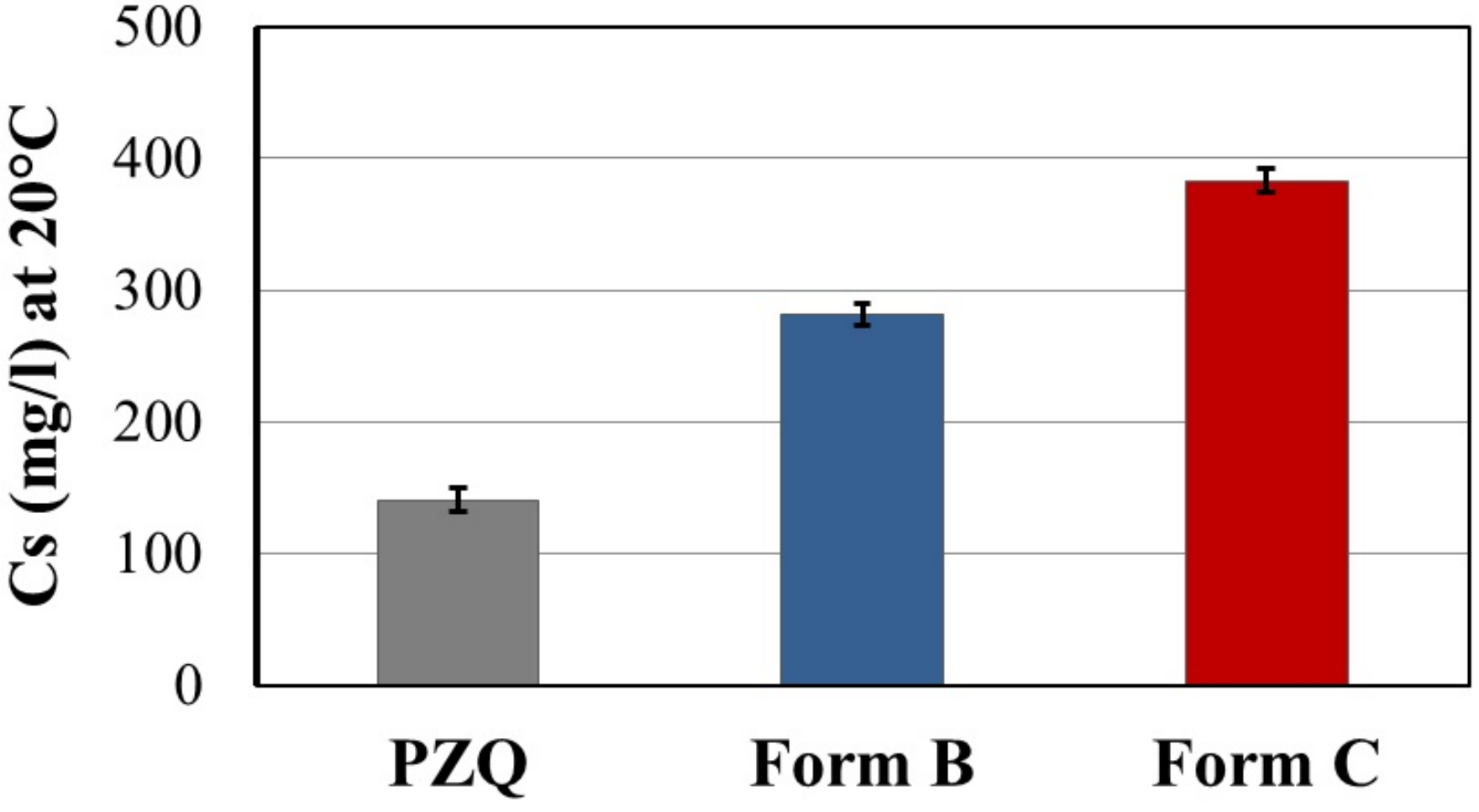
Cs (mg/l) at 20°C
500
400
300
200
100
0
PZQ
Form B
Form C

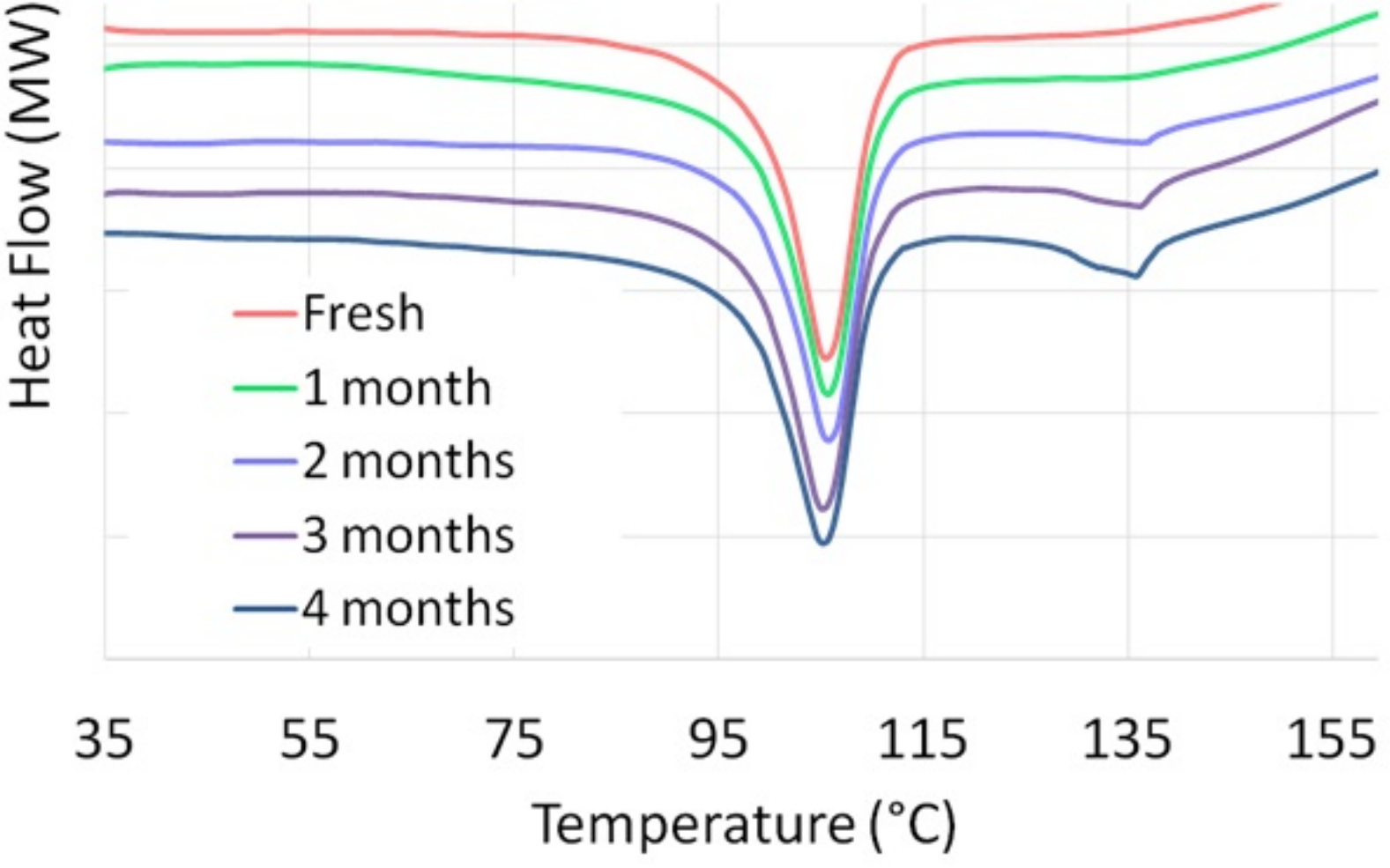
Heat Flow (MW)
Fresh
1 month
2 months
3 months
4 months
35
55
75
95
115
135
155
Temperature (°C)

Supplementary information

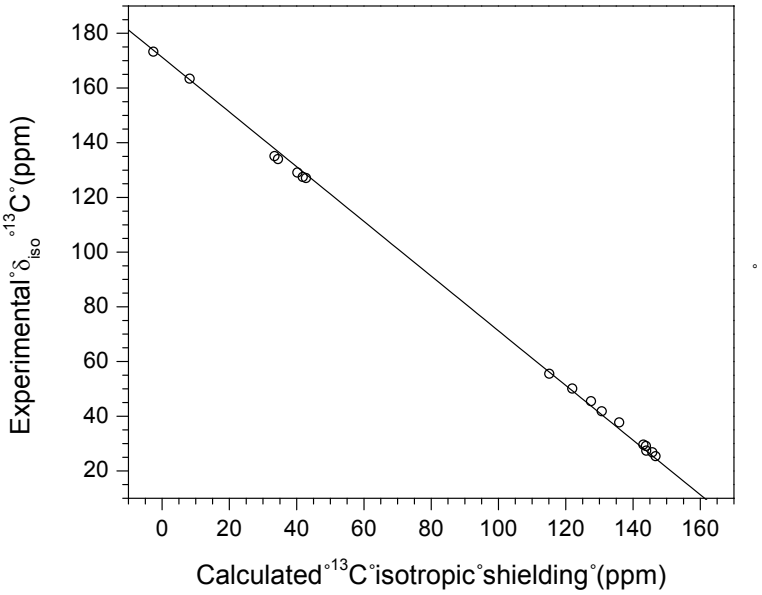

Figure S1. Plot of the experimental ^{13}C chemical shifts against the GIPAW-calculated ^{13}C chemical shieldings (σ_{iso}) to determine σ_{ref}. The slope of the line of best fit was constrained to −1, which gives an intercept of 171.2 ± 0.4 ppm. The Pearson's correlation coefficient is 0.9991.

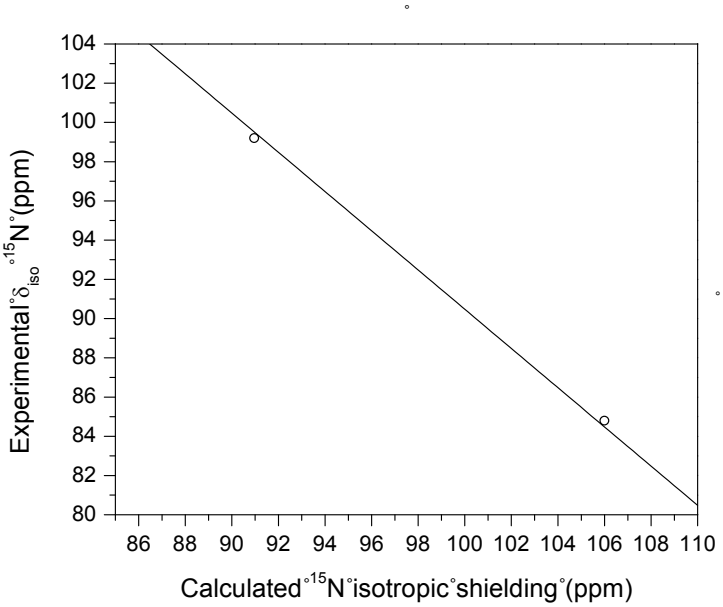

Figure S2. Plot of the experimental ^{15}N chemical shifts against the GIPAW-calculated ^{13}C chemical shieldings (σ_{iso}) to determine σ_{ref}. The slope of the line of best fit was constrained to −1, which gives an intercept of 190.5 ± 0.3 ppm. The Pearson's correlation coefficient is 0.9980.

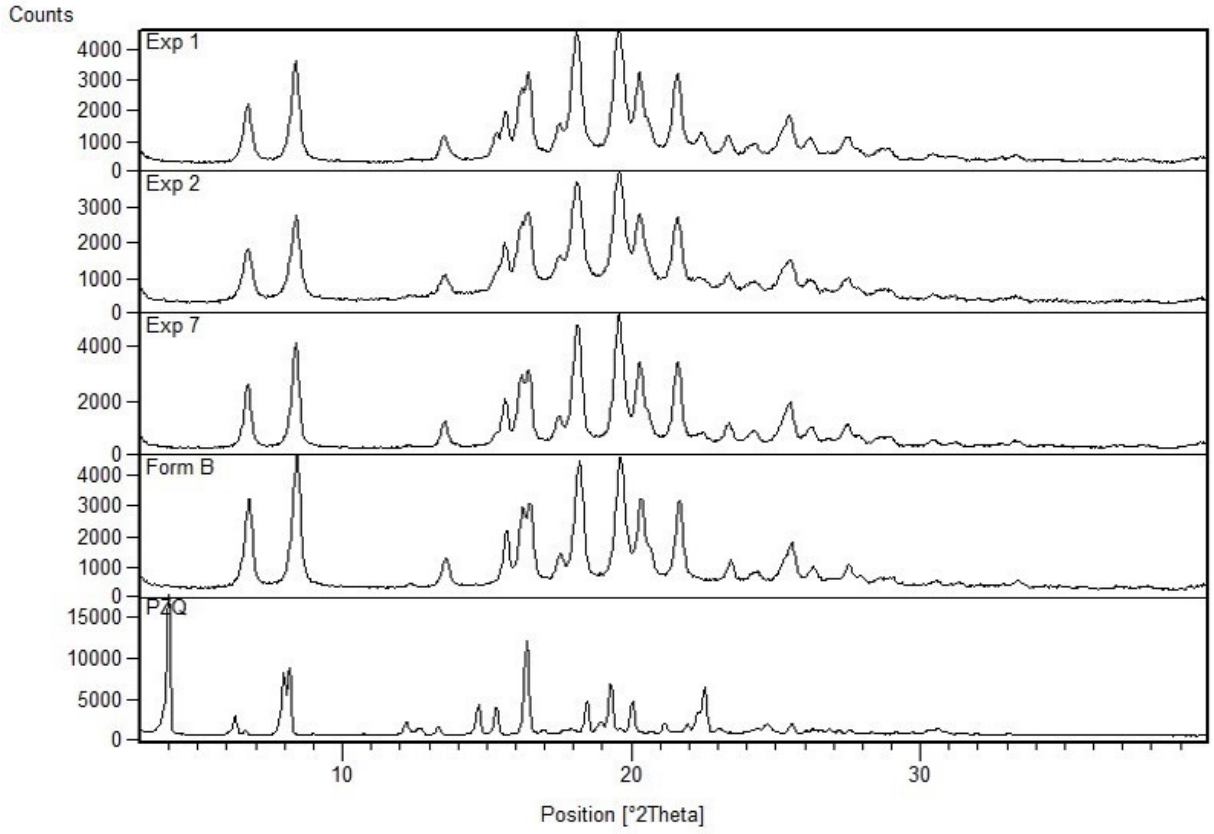

Figure S3a: XRPD patterns of the EXP 1, 2, 7 compared to raw PZQ and Form B.

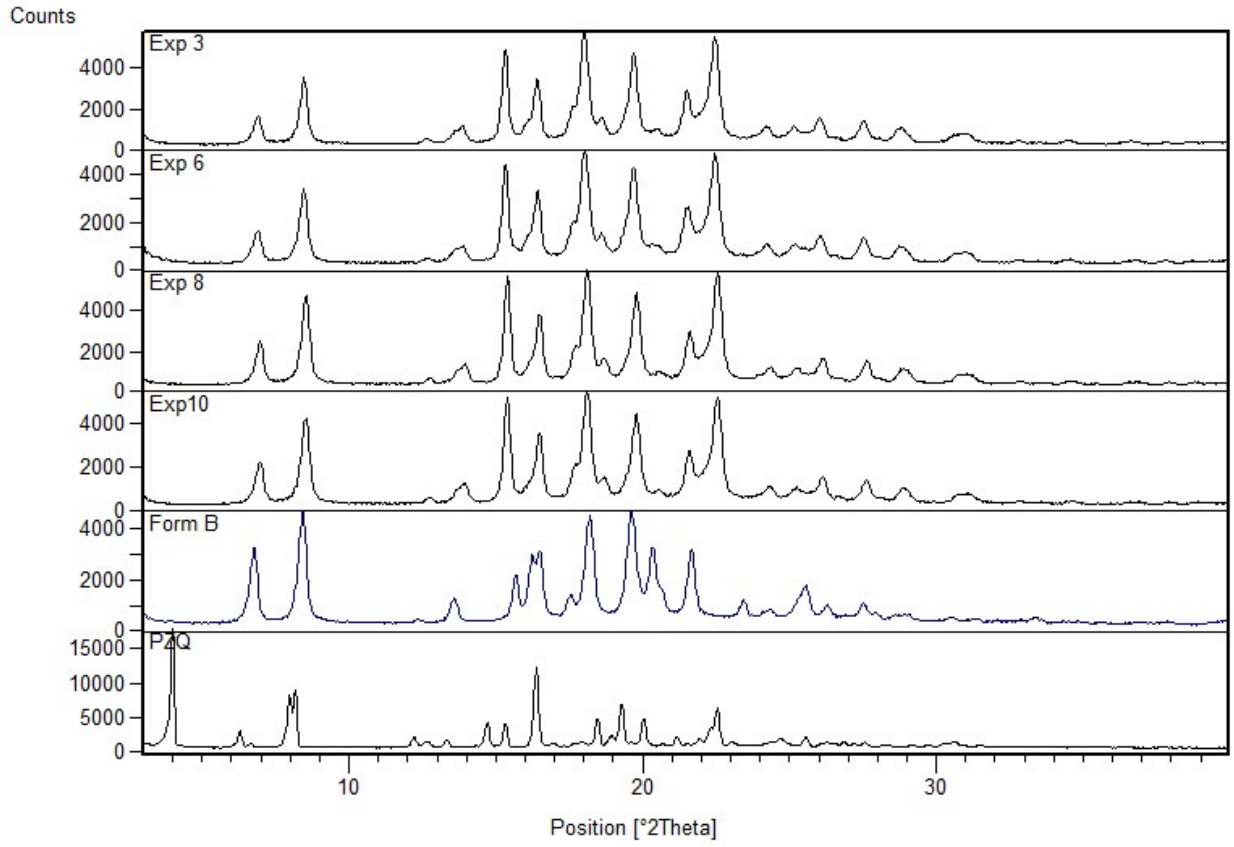

Figure S3b: XRPD patterns of the EXP 3, 6, 8, 10 (Form C), compared to raw PZQ and Form B.

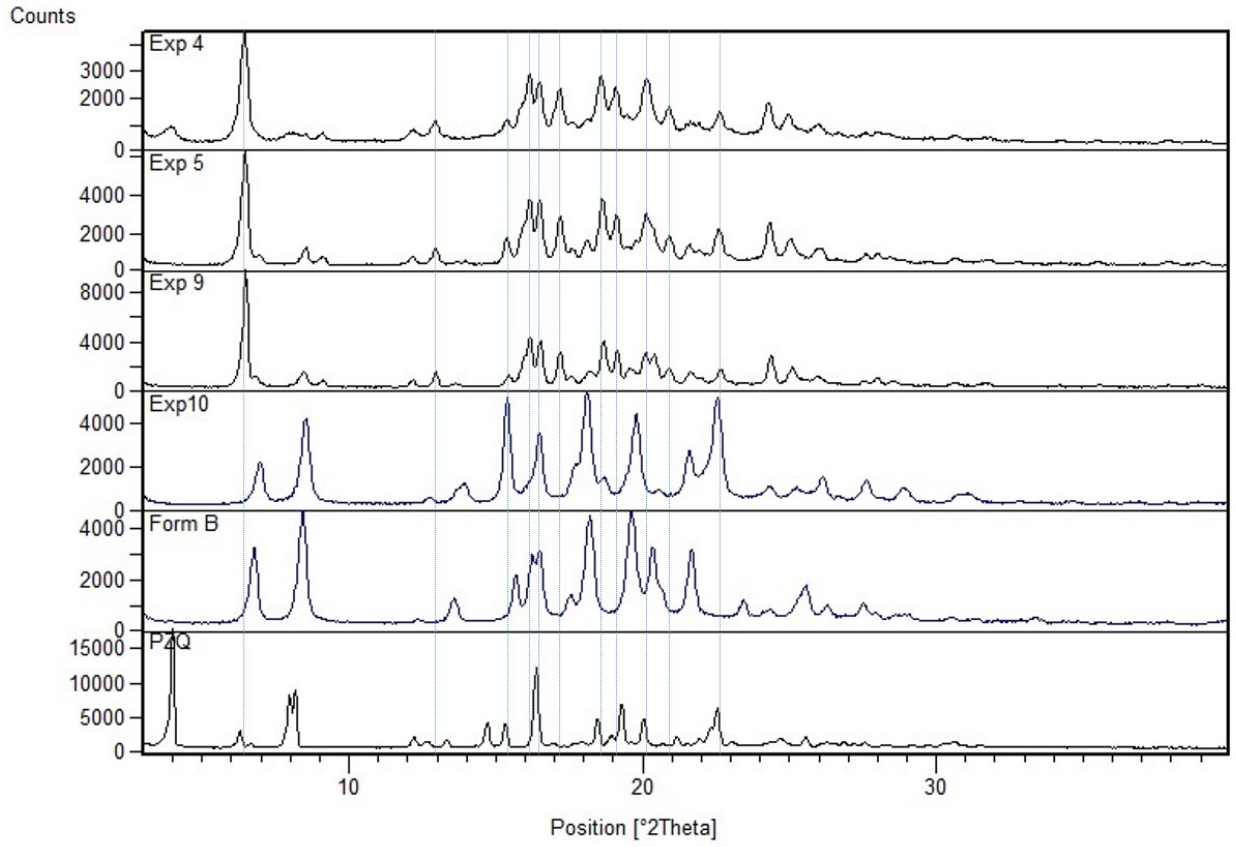

Figure S3c: XRPD patterns of the EXP 4, 5, 9 compared to raw PZQ and Form B and EXP 10 (Form C)

Table S1 : Averaged Results of DSC and TGA analyses of the 10 samples produced in different milling conditions, according to the Doehlert matrix.

EXP	ΔH endothermal event (J/g)	Peak temperature (°C)	Weight loss (%)	Dehydration temperature (°C)
1	62.58	110.51	0.00	-
2	36.39	109.60	0.00	-
3	74.92	106.50	0.00	-
4	4.94	98.62	0.00	-
	86.88	132.81		
5	15.05	70.27	1.35	70
	60.59	109.61		
	8.29	136.76		
6	88.78	134.16	0.00	-
7	63.91	110.34	0.00	-
8	55.64	106.51	0.00	-
9	13.05	74.73	1.35	70
	56.54	111.89		

10	71.06	106.84	0.00	-

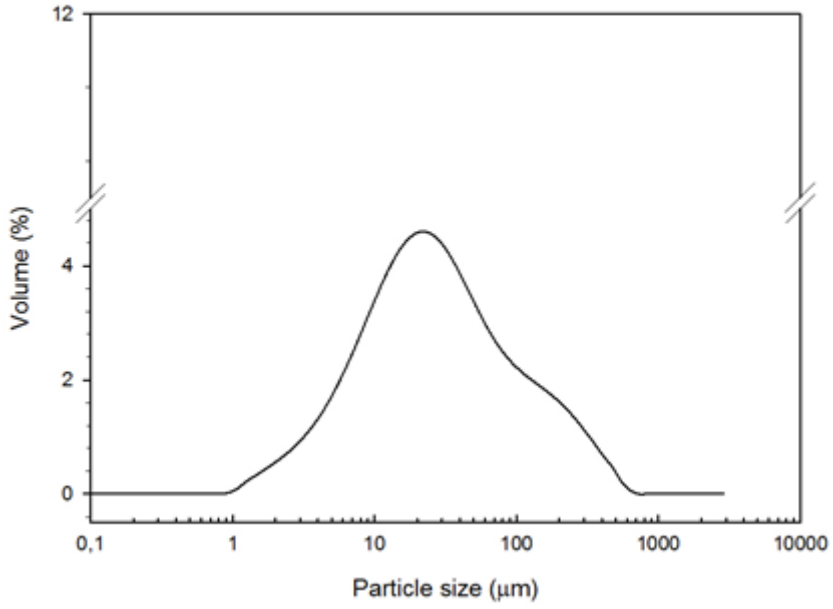

Figure S4. Particle size distribution of raw PZQ

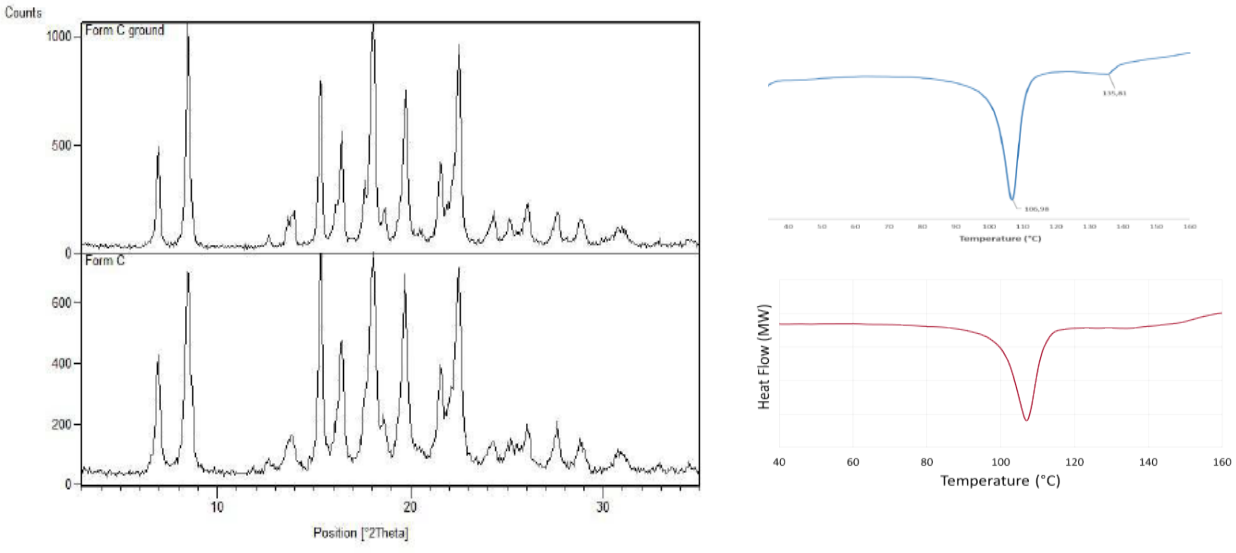

Figure S5. Physical stability of Form C upon milling (60 min at 25 Hz): PXRD pattern (left), and DSC curves (right) of: fresh sample (bottom) and ground sample (up).

Table 1. Doehlert design (2 factors) for neat grinding of PZQ: experimental domain, experimental plan, randomization and responses.

Independent variables		Lower level (coded -1)	Upper level (coded +1)
Milling time (min)	x_1	180	300
Milling frequency (Hz)	x_2	15	25
Dependent variables			
PZQ crystal form*	y_1		
Median particle size (μm)**	y_2		
Drug recovery after milling (%)***	y_3		

Exp.	Random order	X_1	X_2	Milling time (min)	Milling frequency (Hz)	y_1	y_2 (μm) (mean±S.D)	y_3 (%) (mean±S.D.)
1	6	0.966	0.259	298	21	B	68.00±3.29	99.01±0.14
2	2	-0.966	-0.259	182	19	*B*	71.85±5.03	98.32±0.34
3	10	0.259	0.966	256	25	C	55.46±4.01	99.04±0.02
4	3	-0.259	-0.966	225	15	M	40.44±4.57	99.64±0,04
5	9	0.707	-0.707	282	16	M	47.19±3.09	99.32±0.16
6	4	-0.707	0.707	198	24	*C*	58.06±0.48	99.38±0.11
7	1	0.000	0.000	240	20	B	77.44±3.99	99.55±0.05
8	5	-0.433	-0.250	214	19	*C*	54.17±5.22	99.71±0.13
9	7	0.433	-0.250	266	19	M	40.80±0.34	99.16±0.23
10§	**8**	**0.000**	**0.500**	**240**	**23**	**C**	**57.33±3.44**	**99.42±0.10**

*characterized by XRPD analysis and confirmed by DSC and TGA analyses. Letters in italic font indicate a solid product with reduced crystallinity degree (corresponding to ligth colors in Figure 2). The presence of Form B is reported as *B*, Form C as *C*, while *M* correspond to mixtures of different crystalline forms and amorphous solid. ** determined by Laser Light Scattering; *** assessed by HPLC analysis;
§ process conditions taken as the standard ones for Form C

Table 2. Experimental and calculated ^{13}C and ^{15}N isotropic chemical shifts for the polymorph Form C of PZQ, with the corresponding assignments for each site in the asymmetric unit. The GIPAW-calculated chemical shielding are also reported.

Atom	Group	^{13}C		
		δ_{iso}(exp) / ppm	δ_{iso}(calc) / ppm	σ_{iso} / ppm
7’	C=O	173.3	173.8	−2.6
4	C=O	163.4	163.1	8.2
7a	C_q	135.1	137.8	33.4
11a	C_q	134	136.8	34.5
8	$CH_{(ar.)}$	129.1	131.0	40.2
11	$CH_{(ar.)}$	127.5	129.4	41.8
10	$CH_{(ar.)}$	127.1	128.5	42.8
9	$CH_{(ar.)}$	n.a.[a]	127.9	43.4
11b	$CH_{(aliph.)}$	55.5	56.1	115.1
3	CH_2	50.1	49.3	121.9
1	CH_2	45.5	43.8	127.5
1’	$CH_{(aliph.)}$	41.8	40.5	130.7
6	CH_2	37.7	35.3	135.9
2'	CH_2	29.6	28.1	143.1
7	CH_2	29.1	27.4	143.8
6'	CH_2	27.4	27.3	143.9
3'	CH_2	26.8	25.5	145.7
4'5’	CH_2	25.4	24.5	146.7
5'4’	CH_2	n.a.[a]	23.4	147.9
			^{15}N	
2	N	84.8	84.5	106.0
5	N	99.2	99.5	91.0

[a]Resonances are indistiguishable.

checkCIF/PLATON report

Structure factors have been supplied for datablock(s) PZQFormC

THIS REPORT IS FOR GUIDANCE ONLY. IF USED AS PART OF A REVIEW PROCEDURE FOR PUBLICATION, IT SHOULD NOT REPLACE THE EXPERTISE OF AN EXPERIENCED CRYSTALLOGRAPHIC REFEREE.

No syntax errors found. CIF dictionary Interpreting this report

Datablock: PZQFormC

Bond precision: C-C = 0.0122 A Wavelength=0.70000

Cell: a=22.017(15) b=5.910(1) c=26.980(2)
alpha=90 beta=109.765(4) gamma=90
Temperature: 298 K

	Calculated	Reported
Volume	3304(2)	3304(2)
Space group	I 2/c	I2/c
Hall group	-I 2yc	-I 2xc
Moiety formula	C19 H24 N2 O2	C19 H24 N2 O2
Sum formula	C19 H24 N2 O2	C19 H24 N2 O2
Mr	312.40	312.40
Dx,g cm-3	1.256	1.256
Z	8	8
Mu (mm-1)	0.078	0.075
F000	1344.0	336.0
F000’	1344.49	
h,k,lmax	10,2,13	
Nref	208	
Tmin,Tmax		
Tmin’		

Correction method= Not given

Data completeness= 0.000 Theta(max)=

R(reflections)= wR2(reflections)=

S = Npar=

The following ALERTS were generated. Each ALERT has the format
test-name_ALERT_alert-type_alert-level.
Click on the hyperlinks for more details of the test.

Alert level B

PLAT340_ALERT_3_B Low Bond Precision on C-C Bonds ..... 0.01219 Ang.

Alert level C

REFI015_ALERT_1_C _refine_ls_shift/su_max is missing
Maximum shift/s.u. ratio after final refinement cycle.
The following tests will not be performed
SHFSU_01
THETM01_ALERT_3_C The value of sine(theta_max)/wavelength is less than 0.500
Calculated sin(theta_max)/wavelength = 0.4886
PLAT127_ALERT_1_C Implicit Hall Symbol Inconsistent with Explicit -I 2xc
PLAT410_ALERT_2_C Short Intra H...H Contact H11 ..H13 . 1.94 Ang.
x,y,z = 1_555 Check

Alert level G

ABSMU01_ALERT_1_G Calculation of _exptl_absorpt_correction_mu
not performed for this radiation type.
PLAT092_ALERT_4_G Check: Wavelength Given is not Cu,Ga,Mo,Ag,In Ka 0.70000 Ang.
PLAT793_ALERT_4_G Model has Chirality at C11 (Centro SPGR) S Verify
PLAT860_ALERT_3_G Number of Least-Squares Restraints ..... 132 Note

---

0 **ALERT level A** = Most likely a serious problem - resolve or explain
1 **ALERT level B** = A potentially serious problem, consider carefully
4 **ALERT level C** = Check. Ensure it is not caused by an omission or oversight
4 **ALERT level G** = General information/check it is not something unexpected

3 ALERT type 1 CIF construction/syntax error, inconsistent or missing data
1 ALERT type 2 Indicator that the structure model may be wrong or deficient
3 ALERT type 3 Indicator that the structure quality may be low
2 ALERT type 4 Improvement, methodology, query or suggestion
0 ALERT type 5 Informative message, check

It is advisable to attempt to resolve as many as possible of the alerts in all categories. Often the minor alerts point to easily fixed oversights, errors and omissions in your CIF or refinement strategy, so attention to these fine details can be worthwhile. In order to resolve some of the more serious problems it may be necessary to carry out additional measurements or structure refinements. However, the purpose of your study may justify the reported deviations and the more serious of these should normally be commented upon in the discussion or experimental section of a paper or in the "special_details" fields of the CIF. checkCIF was carefully designed to identify outliers and unusual parameters, but every test has its limitations and alerts that are not important in a particular case may appear. Conversely, the absence of alerts does not guarantee there are no aspects of the results needing attention. It is up to the individual to critically assess their own results and, if necessary, seek expert advice.

Publication of your CIF in IUCr journals

A basic structural check has been run on your CIF. These basic checks will be run on all CIFs submitted for publication in IUCr journals (*Acta Crystallographica, Journal of Applied Crystallography, Journal of Synchrotron Radiation*); however, if you intend to submit to *Acta Crystallographica Section C* or *E* or *IUCrData*, you should make sure that full publication checks are run on the final version of your CIF prior to submission.

Publication of your CIF in other journals

Please refer to the *Notes for Authors* of the relevant journal for any special instructions relating to CIF submission.

PLATON version of 18/02/2019; check.def file version of 18/02/2019

Datablock PZQFormC - ellipsoid plot